https://doi.org/10.5194/egusphere-2026-4452
Preprint. Discussion started: 28 July 2026

Oxygen Dynamics in Intertidal Sediments: Integrating High-Resolution Data and Reaction-Transport Modeling

Qi Liu[1,2], Karline Soetaert[1], Lucille Hoogerdijk[2], Valle Perez-Rodriguez[3], and Lubos Polerecky[2]

[1]Department of Estuarine and Delta Systems, Royal Netherlands Institute for Sea Research (NIOZ), Yerseke, The Netherlands
[2]Department of Earth Sciences, Faculty of Geosciences, Utrecht University, Utrecht, The Netherlands
[3]Biodiversity and Ecosystem Functioning Laboratory, Department of Biology, Instituto Universitario de Investigación Marina (INMAR), Universidad de Cádiz, Puerto Real, Cádiz, Spain

Correspondence: Qi Liu (qi.liu@nioz.nl)

Abstract. Predicting the response of O_2 dynamics in intertidal sediments to changing environmental conditions is essential for understanding and forecasting the impacts of climate change on coastal biogeochemical functioning. However, key environmental controls such as light, temperature and tidal regime (immersion vs. emersion) are only partially integrated into existing sediment biogeochemical models. Additionally, inversion-based approaches, which infer reaction rates from measured O_2 profiles without explicitly representing the underlying diagenetic mechanisms, cannot be used predictively. We developed a reaction-transport model for simulating O_2 dynamics in MPB-inhabited intertidal sediments at high spatial and temporal resolution under variable environmental forcing. The model was constrained and evaluated using laboratory microsensor measurements of O_2 concentrations and gross photosynthesis in muddy sediments from the Oosterschelde tidal bay (the Netherlands). Our analysis indicates that the studied MPB community is adapted to low irradiance and responds to changing light conditions through vertical migration. Reoxidation of reduced inorganic substances dominates sediment O_2 consumption at low irradiance, whereas aerobic mineralization becomes increasingly important at higher irradiance, with photorespiration representing an additional relevant O_2 sink under high-irradiance conditions. Additionally, both the O_2 producing and consuming processes show strong immersion-emersion and temperature response. Overall, the model is released as an open-source tool, providing a framework that can be adapted and refined for interpreting and predicting O_2 dynamics in intertidal systems under a broad range of environmental conditions.

1 Introduction

Coastal sediments, including intertidal flats, are vital centers for organic matter mineralization and nutrient recycling (Rios-Yunes et al., 2023). The upper sediment layers act as biogeochemical hotspots, supporting more chemical processes than the entire overlying water column (Boudreau and Jørgensen, 2001). Dissolved molecular oxygen (O_2) is the most favorable electron acceptor available in sediments and a key factor that regulates other biogeochemical processes (Glud, 2008). In the future, coastal benthic ecosystems, particularly intertidal flats, are projected to face increasing stressors such as warming, sea-level rise, and altered organic matter inputs (Hewitt et al., 2016; Liu et al., 2025), all of which can strongly influence sediment O_2 availability. Therefore, a deeper understanding of sediment O_2 dynamics is essential to make robust predictions about the

https://doi.org/10.5194/egusphere-2026-4452
Preprint. Discussion started: 28 July 2026

impacts of climate change on coastal benthic environments, including those associated with deoxygenation and increasingly frequent marine heatwaves (Giomi et al., 2023). One possible approach to achieve this is by developing models of the most relevant O_2 producing and consuming processes in sediments and their dependence on environmental variables.

In intertidal sediments, O_2 is produced via photosynthesis by microorganisms commonly called microphytobenthos (MPB), while O_2 losses occur mainly through organic matter mineralization by benthic organisms and aerobic bacteria, as well as through microbially mediated oxidation of reduced inorganic species (Santschi et al., 1990). These O_2 production and consumption processes are temperature dependent and therefore dynamically change due to temperature fluctuations (Hancke and Glud, 2004). Because light regulates MPB eco-physiology (e.g., photoacclimation and photoinhibition) and induces circadian rhythms of vertical migration (Baklouti et al., 2006; Han, 2002), O_2 production additionally varies due to fluctuations in available light. Furthermore, O_2 production by MPB is impacted by tidal inundation, which alters the amount of solar radiation reaching the sediment surface, rapidly modifies sediment temperature, and reshapes nutrient availability (Liu et al., 2025). As a result of these dependencies, O_2 availability in intertidal areas is dynamically changing over timescales ranging from seconds to seasons.

Presently, models capable of predicting O_2 dynamics in intertidal sediments on these widely ranging time scales do not exist. However, evidence from similar models developed for other marine productive ecosystems (i.e., coral reefs, seagrass meadows and mangrove forests) suggests that focusing primarily on large-scale temporal averages, while overlooking small-scale fluctuations, may yield inaccurate predictions for O_2 availability (Giomi et al., 2023; Fusi et al., 2023). In this study, we make the first step towards a model that can predict MPB-driven O_2 dynamics in intertidal sediments on fine spatial scales and both short and long temporal scales.

Until now, attempts to model MPB-related processes have largely focused on specific processes in isolation (Nmor, 2020), such as migratory rhythms (Serôdio and Catarino, 2000), trophic interactions (Blackford, 2002), light and tidal influences (Savelli et al., 2018), hydrodynamics (Mariotti and Fagherazzi, 2012), and behavioral and physiological adaptations (Guarini et al., 2000), rather than considering their combined effects on sediment biogeochemistry. While some modeling studies integrate MPB photosynthesis and nutrient uptake with sediment biogeochemical profiles, they exclude MPB vertical migration in response to light, which can strongly alter O_2 production and vertical gradients and thereby influence sediment biogeochemical profiles, or do not capture biogeochemistry at fine spatial resolutions (Rakotomalala et al., 2019; Hochard et al., 2010). Additionally, while some models account for temperature effects on MPB production (Guarini et al., 2000; Savelli et al., 2018), they do not extend this to the full range of O_2-related biogeochemical reactions, potentially biasing predictions under warming conditions.

Attempts to quantify MPB primary production have, for a long time, adapted 'pelagic' approaches, such as incubations with isotopically labeled (^{13}C or ^{14}C) dissolved inorganic carbon, light-dark incubations combined with O_2 measurements, or methods based on variable Chl *a* fluorescence (Barranguet et al., 1998; Kromkamp and Forster, 2003). However, transferring these techniques to benthic systems is challenging because of steep, millimeter-scale biogeochemical gradients in the euphotic zone caused by the high concentration of biomass, strong light attenuation, and mass transfer limitation in sediments. To overcome these challenges, the development of high-resolution, rapid-response tools such as O_2 microelectrodes (Revsbech,

https://doi.org/10.5194/egusphere-2026-4452
Preprint. Discussion started: 28 July 2026

1989) and fiber-optic based irradiance microprobes (Jørgensen and Des Marais, 1986; Lassen et al., 1992) has enabled detailed measurements of chemical (O_2 concentration) and physical (light) microenvironments within MPB communities (Revsbech and Jørgensen, 1983; Kühl and Jørgensen, 1992, 1994). Several studies have applied these methods to investigate how key environmental drivers, such as temperature (Hancke and Glud, 2004), light intensity (Al-Najjar et al., 2012; Haro et al., 2019a; Meresse et al., 2023), and immersion/emersion conditions (Haro et al., 2019b) influence the energy and O_2 budgets in benthic systems.

Although microsensors are very useful for probing highly stratified systems, the data they generate require careful interpretation. To date, most efforts to interpret microsensor profiles have relied on inverse or numerical procedures that estimate depth-resolved net production and consumption rates from observed gradients (Berg et al., 1998). While powerful for constraining local net budgets, these methods are essentially diagnostic and lack explicit mechanistic representation of the underlying diagenetic pathways. As a result, they cannot be used predictively to evaluate how O_2 dynamics respond to changes in environmental forcing.

To address the limitations identified above, we present a model for predicting O_2 dynamics in MPB-inhabitted intertidal sediments on fine spatial and temporal scales. The model integrates mechanistic and empirical formulations to describe the underlying processes (i.e., O_2 production and consumption and transport) and components (e.g., MPB biomass) controlling system dynamics, including their response to temperature, light, and sediment emersion. Presently, the model only considers diffusive transport and is therefore applicable to systems such as muddy sediments, where other transport mechanisms can be neglected. Additionally, we present microsensor-based data used to calibrate the model. The data were acquired from sediment samples collected in the Oosterschelde tidal bay and include vertical profiles of steady-state O_2 concentrations and gross rates of photosynthetic O_2 production (GPP) measured with a high spatial resolution under varying temperature, light, and immersion/emersion conditions. Overall, the model provides a predictive quantitative tool for assessing O_2-related process rates and budgets in muddy intertidal sediments, laying a foundation for future studies on benthic ecology and biogeochemistry of these systems.

2 Materials and Methods

In this section, we first describe the laboratory experiments, including sediment sampling, setup, and microsensor measurements. Then, we explain the mathematical formulation and numerical implementation of the model. Finally, we describe the model calibration strategy and present key model outcomes. This structure reflects the workflow of the study, where experimental observations form the foundation for model development, calibration, and evaluation.

https://doi.org/10.5194/egusphere-2026-4452
Preprint. Discussion started: 28 July 2026

2.1 Laboratory experiments

2.1.1 Sampling

Surficial sediments were sampled from intertidal flats in the Oosterschelde tidal bay, located in the southwest of the Netherlands. The sampling station ZK1 was chosen for its high MPB biomass and relatively low levels of animal disturbance. The sediments in this location are inundated twice daily and experience large fluctuations in temperature and solar radiation (Liu et al., 2025). More detailed description of the sediments is provided in Borger et al. (2020) and Rios-Yunes et al. (2023).

Sediment samples were collected during low tides between September 2023 and March 2024 by inserting a transparent cylindrical PVC tube (15 cm in diameter and 30 cm in height) into the sediment and carefully extracting it to avoid surface disturbance. Additionally, 20 L of seawater was collected near the sampling site. Both sediment and water samples were immediately transported to the laboratory at NIOZ, Yerseke, where they were incubated in a thermostatic bath inside a climate-controlled room at a temperature matching the value determined *in situ* during sample collection. Microsensor measurements started the following day.

2.1.2 Experimental setup and design

The experimental setup and measurement protocols used in the present study were similar to those previously described by Al-Najjar et al. (2010). Briefly, measurements were conducted in sediment cores placed in a transparent glass aquarium. A chiller/heater circulator was used for controling the water temperature, a tube connected to a pump for adjusting the water level, and a lamp with adjustable luminance as a light source (Fig. **S1**). Further technical details about the setup are provided in Supplementary Methods.

The general experimental approach involved two types of measurements. First, a light microsensor was used to characterize the vertical light distribution in the sediment. Subsequently, an O_2 microsensor was used to quantify the corresponding photosynthetic activity of MPB and the vertical distribution and dynamics of O_2. Light and O_2 measurements were conducted separately, always using a new (intact) sediment core. This approach was necessary to avoid interference between the sensors and minimize changes in the MPB biomass distribution in the sediment possibly occurring during the lengthy measurements.

Three separate experiments were conducted to quantify the effects of light, temperature, and tidal inundation on the MPB activity and the resulting sediment O_2 dynamics: a photosynthesis–irradiance (PI), temperature ramping (TR), and immersion–emersion (IE) experiment. In each experiment, only one environmental factor was varied while the others were held constant. The variation imposed on the irradiance and temperature was based on the range observed in the field (see Table **S1** for details). To estimate variability among the sediment samples, each experiment was conducted in three replicate cores. In one replicate core of the TR experiment, the ambient temperature was additionally decreased to the starting value after ramping to examine potential recovery of the photosynthetic O_2 production following inhibition at high temperature.

At the end of each experiment, salinity of the overlying water was measured, followed by the collection of three MPB biofilm samples from the sediment surface (area 1 cm^2, thickness 2–3 mm) for Chl-*a* quantification. The Chl-*a* content was determined in µg Chl-*a*/g of sediment and converted to $mol\,C/m^2$ (Table **S2**). The conversion used the carbon-to-chlorophyll-*a*

https://doi.org/10.5194/egusphere-2026-4452
Preprint. Discussion started: 28 July 2026

ratio of $100\,\mathrm{g\,C/g\,Chl\text{-}}a$, which is representative of estuarine benthic diatom populations in the summer under high-light and high-temperature conditions (De Jonge, 1980; Cloern et al., 1995).

2.1.3 Light microsensor measurements

Vertical light distribution in the sediment was measured using a fiber-optic scalar irradiance microprobe (Lassen et al., 1992). The microprobe had a spherical measuring tip (diameter of about $80\,\mu\mathrm{m}$) attached to a tapered optical fiber connected to a spectrometer, allowing quantification of spectrally resolved total radiant flux from all directions around the measurement point. Measurements were conducted in vertical steps of $100\,\mu\mathrm{m}$, starting from the overlying water and continuing into the sediment until no signal was detectable. At each depth, three replicate spectra were recorded and averaged. The mean signal between 800–$1000\,\mathrm{nm}$ was then subtracted from each spectrum to account for sensor offset, followed by spectral integration across the range of photosynthetically active radiation (PAR, 400–$700\,\mathrm{nm}$). The spectrally corrected and integrated values determined at each depth were then normalized to the value measured at the sediment surface. To estimate spatial heterogeneity, light profiles were measured in three sediment cores, at five randomly selected locations per core.

2.1.4 O_2 microsensor measurements

O_2 concentrations were measured using a fast-response Clark-type microelectrode (Revsbech, 1989). The microsensor (tip diameter: $50\,\mu\mathrm{m}$, response time: $\sim 0.5\,\mathrm{s}$) was calibrated using a linear, two-point calibration with $100\,\%$ air-saturated and anoxic seawater, accounting for experimental temperature and salinity. Each measurement began by setting the incident irradiance to a constant value. The O_2 microsensor tip was then positioned about 1–$2\,\mathrm{mm}$ above the sediment surface. After 15 minutes, two vertical O_2 profiles were measured in $50\,\mu\mathrm{m}$ steps until a depth where no O_2 was detected. Once these measurements confirmed that a steady state was reached, GPP rates were measured in $100\,\mu\mathrm{m}$ steps using the light-dark shift method (Revsbech and Jørgensen, 1983). Briefly, the microsensor tip was positioned at the target depth and the sensor signal was allowed to stabilize. The incident light was then abruptly blocked with an opaque black plastic sheet, which led to a rapid decrease in O_2 concentrations, and then restored to the original value by removing the sheet after 2–$3\,\mathrm{s}$. The slope of the linear decrease in O_2 concentration during the dark interval, following immediately (within $0.5\,\mathrm{s}$) the moment of light removal, was calculated and taken as the rate of GPP at that depth. The GPP measurements were repeated at progressively greater depths until the light removal led to no detectable immediate decrease in O_2 concentrations. After completing the GPP measurements, the system was allowed to recover and two additional O_2 profiles were measured to verify steady state. Depending on the experiment (PI, TR, or IE), these measurements were repeated using different levels of incident irradiance, water temperature, or water height above the sediment surface (Table **S1**).

https://doi.org/10.5194/egusphere-2026-4452
Preprint. Discussion started: 28 July 2026

2.2 Numerical model

2.2.1 Spatial domain

For a submerged sediment, the modeled vertical domain comprises two layers: a thin water column on top of a sediment column. Depth, denoted by z, extends from $-z_{\mathrm{DBL}}$ in the water to z_{sed} in the sediment and equals to 0 at the sediment-water interface (SWI). Here, z_{DBL} denotes the thickness of the diffusive boundary layer (DBL), which is a thin water layer directly above the sediment surface where molecular diffusion dominates solute transport due to suppressed turbulence (Boudreau and Jørgensen, 2001), while z_{sed} is the thickness of the sediment layer. The model domain is discretized into a grid comprising 20 layers in the water column and 280 layers in the sediment. For both grids, the thickness of the grid cells increases geometrically with depth from $1\,\mu\mathrm{m}$ in the uppermost grid cell. The two grids are coupled at the SWI through continuity of concentrations and diffusive fluxes. For a sediment exposed to air, the vertical domain has the same structure and dimensions but the water layer is replaced with a layer of air, achieved by changing the corresponding diffusion coefficient (see below).

2.2.2 Governing equations

The model includes two state variables: dissolved O_2 and oxygen demand units (ODU). ODU represents the lumped concentration of reduced dissolved substances (e.g., ammonium, sulfide, reduced iron) that can react with O_2 through reoxidation reactions (Soetaert et al., 1996). Concentrations of both solutes are expressed in moles of O_2 per unit volume of porewater ($\mathrm{mol\,O_2/m^3_{pw}}$) and denoted by C_i, with $i = O_2$ or ODU. The modeled system is assumed to be laterally homogeneous, with transport governed solely by molecular diffusion. Accordingly, the concentration dynamics for both solutes are described by a one-dimensional diffusion–reaction equation,

$$\frac{\partial C_i}{\partial t} = \frac{1}{\theta} \cdot \frac{\partial}{\partial z}\left(\theta \cdot D_i \cdot \frac{\partial C_i}{\partial z}\right) + R_i, \tag{1}$$

where t denotes time (in days), θ denotes porosity, i.e., the volume of porewater per volume of bulk sediment ($\mathrm{m^3_{pw}/m^3}$), D_i is the diffusion coefficient ($\mathrm{m^2\,d^{-1}}$), and R_i is the net reaction rate, expressed per unit volume of porewater ($\mathrm{mol\,O_2/m^3_{pw}/d}$).

In general, all quantities in this equation (except for time) vary with z. To account for the two-layer domain structure, porosity is modeled by a function varying between 1 in the water column and 0.9 in the sediment, with a sharp exponential transition below the SWI (Fig. **S2**). For a submerged sediment, the diffusion coefficient for the component i is calculated according to $D_i = D_{i,mol}/(1 - \ln\theta^2)$, where $D_{i,mol}$ is the molecular diffusion coefficient in seawater and the factor in the denominator accounts for sediment tortuosity (only relevant in the sediment, i.e., for $\theta < 1$). The dependence of $D_{i,mol}$ on temperature and salinity is accounted for and calculated with the R package `marelac` (Soetaert et al., 2010a). The diffusion coefficient for H_2S is taken as a representative value of D_{mol} for ODU. When modeling the sediment exposed to air, the value of $D_{i,mol}$ in the air layer (i.e., for $-z_{\mathrm{DBL}} \leq z < 0$) is replaced by the corresponding diffusion coefficient of the component i in air, while the value of $D_{i,mol}$ in seawater is retained when calculating D_i in the sediment layer (i.e., for $z_{\mathrm{sed}} \geq z \geq 0$). Since diffusion

https://doi.org/10.5194/egusphere-2026-4452
Preprint. Discussion started: 28 July 2026

of gases in air is roughly 10^4-fold faster in air than in water (Cussler, 2009), this replacement effectively compresses the DBL thickness to zero and yields no variation in the O_2 and ODU concentration within the air layer.

By definition, the reaction rates are zero in the water or air column above the sediment surface and non-zero inside the sediment. For O_2, the net reaction rate is partitioned between processes that contribute to O_2 production and consumption, including MPB photosynthesis ($R_{photosyn}$), basal respiration ($R_{basalresp}$) and photorespiration ($R_{photoresp}$), aerobic mineralization of photosynthetically produced organic carbon, driven by microorganisms associated with MPB ($R_{aeromin}$), and ODU reoxidation (R_{reox}). Thus, the net rate is expressed as a sum

$$R_{O_2} = R_{photosyn} - R_{basalresp} - R_{photoresp} - R_{aeromin} - R_{reox}. \tag{2}$$

In contrast, the reaction rate for ODU is assumed to only comprise the contribution from ODU reoxidation,

$$R_{ODU} = -R_{reox}. \tag{3}$$

Regulation of these process rates by environmental variables is described below. The differential equations (Eq. 1) are solved using a fixed concentration and flux at the upper and lower boundary for O_2, respectively, and fixed concentrations at both boundaries for ODU (see more details in Supplementary Methods).

2.2.3 MPB biomass distribution

The model assumes several processes to be driven, directly or indirectly, by the activity of MPB. To account for this, the corresponding process rates are assumed to be proportional to the concentration of active MPB biomass. This concentration is denoted as C_{MPB} and expressed in moles of C per unit volume of bulk sediment ($\mathrm{mol\,C/m^3}$). To allow some flexibility in the vertical distribution of the biomass, in particular to allow modeling of redistribution of the biomass by migration in response to environmental stimuli such as light, C_{MPB} is formulated as an explicit function of depth in the sediment. In the present model, this function is assumed to follow a truncated normal distribution, i.e.,

$$C_{MPB}(z) = B_{\mathrm{MPB}} \cdot \frac{1}{\sigma} \cdot \frac{\phi\left(\frac{z-\mu}{\sigma}\right)}{1-\Phi\left(\frac{-\mu}{\sigma}\right)} \quad \text{for } z \geq 0, \tag{4}$$

and $C_{MPB}(z) = 0$ for $z < 0$. In this expression, ϕ denotes the probability density function (PDF) of the standard normal distribution, Φ is the corresponding cumulative distribution function (CDF), and μ and σ (both in m) describe the vertical position of the peak MPB biomass and degree of dispersion, respectively. The normalization factor $1-\Phi\left(\frac{-\mu}{\sigma}\right)$ in the denominator ensures that the depth integral of $C_{\mathrm{MPB}}(z)$ over the sediment domain is equal to B_{MPB}, which is the total active MPB biomass per $\mathrm{m^2}$ of sediment (in $\mathrm{mol\,C/m^2}$).

https://doi.org/10.5194/egusphere-2026-4452
Preprint. Discussion started: 28 July 2026

2.2.4 Regulation of process rates

The model assumes the following regulation of the process rates by environmental variables. The rate of photosynthetic O_2 production at depth z in the sediment is proportional to the local concentration of the active MPB biomass and controlled by the locally available light, $I(z)$, and height of the water column above the sediment surface, h:

$$R_{photosyn}(z) = r_{photosyn} \cdot \frac{C_{\mathrm{MPB}}(z)}{\theta} \cdot f(I(z)) \cdot g(h). \tag{5}$$

In this expression, $r_{photosyn}$ is the rate coefficient of MPB photosynthesis ($\mathrm{mol\,O_2/mol\,C/d}$), while the functions f and g (both unitless) describe the response of MPB photosynthesis to light and sediment emersion, respectively. The division by θ ensures that the rate is expressed per $\mathrm{m^3_{pw}}$, as required.

The light response of MPB photosynthesis is assumed to follow the relationship proposed by Eilers and Peeters (1988),

$$f(I) = \frac{2 \cdot (1+w) \cdot \left(\frac{I}{k_I}\right)}{\left(\frac{I}{k_I}\right)^2 + 2 \cdot w \cdot \left(\frac{I}{k_I}\right) + 1}, \tag{6}$$

where I is the intensity of available light, k_I is the light intensity where photosynthesis reaches the highest value (both in $\mathrm{\mu mol\ photons/m^2/s}$), and w determines the shape of the light response curve (i.e., the initial slope and degree of photoinhibition).

As indicated in Eq. 5, O_2 production at depth z is controlled by the locally available irradiance, $I(z)$. In line with previous studies (Kühl and Jørgensen, 1994; Kühl et al., 1994; Al-Najjar et al., 2010), this value is estimated assuming that light attenuates exponentially with depth in the sediment,

$$I(z) = I_0 \cdot \exp\left(-k_{\mathrm{ext}} \cdot z\right), \tag{7}$$

where I_0 is the irradiance at the SWI and k_{ext} ($\mathrm{m^{-1}}$) denotes the light attenuation coefficient of the bulk sediment. The latter value is calculated as a weighted average of light attenuation in the porewater and in the solid fraction of the sediment, $k_{\mathrm{ext}} = \theta \cdot k_{\mathrm{ext,pw}} + (1-\theta) \cdot k_{\mathrm{ext,solid}}$, and as such depends on porosity.

To represent the effect of sediment emersion on MPB photosynthesis, the model uses a heuristic function,

$$g(h) = g_0 + (1-g_0) \cdot \frac{h^2}{h^2 + k_h^2}, \tag{8}$$

where k_h is the water-height limitation constant (m). This function rapidly decreases from 1 to g_0 ($0 < g_0 < 1$) as the sediment surface changes from a submerged ($h > 0$) to an air-exposed ($h = 0$) state (Fig. **S3**).

https://doi.org/10.5194/egusphere-2026-4452
Preprint. Discussion started: 28 July 2026

The rate of MPB basal respiration is assumed to be independent of light conditions, proportional to the MPB biomass, and limited by O_2 availability via a Michaelis–Menten-like regulation,

$$R_{basalresp}(z) = r_{basalresp} \cdot \frac{C_{\mathrm{MPB}}(z)}{\theta} \cdot \frac{C_{O_2}}{C_{O_2} + k_{basalresp}}, \tag{9}$$

where $r_{basalresp}$ (d^{-1}) is the rate coefficient and $k_{basalresp}$ ($\mathrm{mol\,O_2/m^3_{pw}}$) is the corresponding half-saturation concentration. Note that although C_{O_2} is a function of depth, z, this dependency is, for simplicity, not included in the above expression. A similar convention is followed below.

The rate of aerobic mineralization, which is driven by microorganisms that feed on organic carbon produced by MPB photosynthesis, is assumed to be proportional to the rate of organic carbon production (i.e., $R_{photosyn}$) and limited by O_2 availability via a Michaelis–Menten-like regulation,

$$R_{aeromin}(z) = c_{aeromin} \cdot R_{photosyn}(z) \cdot \frac{C_{O_2}}{C_{O_2} + k_{aeromin}}, \tag{10}$$

where $c_{aeromin}$ (unitless) is the fraction of the photosynthetically produced carbon that is mineralized by MPB-associated microbes when O_2 is not limiting and $k_{aeromin}$ ($\mathrm{mol\,O_2/m^3_{pw}}$) is the corresponding half-saturation concentration.

The rate of ODU reoxidation is assumed to be first-order with respect to ODU and limited by O_2 availability via a Michaelis–Menten-like regulation,

$$R_{reox}(z) = r_{reox} \cdot C_{ODU} \cdot \frac{C_{O_2}}{C_{O_2} + k_{reox}}, \tag{11}$$

where r_{reox} (d^{-1}) is the rate coefficient and k_{reox} ($\mathrm{mol\,O_2/m^3_{pw}}$) is the corresponding half-saturation concentration. For simplicity, ODU reoxidation in the overlying water is neglected in the model, i.e., $R_{reox}(z) = 0$ for $z < 0$.

Preliminary model simulations based on the O_2 producing and consuming processes described above led to O_2 concentrations that systematically overestimated the measured values (data not shown). To avoid this bias, photorespiration was included in the model as an additional process responsible for O_2 consumption. This process becomes increasingly important under high O_2 concentrations (which are typical in highly active MPB biofilms) because the carbon-fixing enzyme complex shifts part of its activity towards oxygenation reactions rather than CO_2 assimilation, leading to O_2 removal (Glud et al., 1992; Kühl et al., 1996). The rate of this process was modeled according to

$$R_{photoresp}(z) = c_{photoresp} \cdot R_{photosyn}(z) \cdot \left(\frac{C_{O_2}}{C_{O_2}^{max}} \right)^m, \tag{12}$$

where $C_{O_2}^{max}$ is the air-saturated O_2 concentration at a specific temperature and salinity, m is the reaction order, and $c_{photoresp}$ (unitless) represents the fraction of photosynthetically produced O_2 that is removed by photorespiration when O_2 concentration reaches air saturation, i.e., at $C_{O_2} = C_{O_2}^{max}$. This formulation reflects the strong non-linear increase in photorespiration under supersaturated O_2 conditions, as previously observed in microsensor studies of photosynthetic microbial mats and biofilms

https://doi.org/10.5194/egusphere-2026-4452
Preprint. Discussion started: 28 July 2026

(Glud et al., 1992; Kühl et al., 1996). Additionally, it is consistent with the empirical relationship derived from experiments showing that photorespiratory O_2 uptake increases proportionally with photosynthetic O_2 production and becomes increasingly significant only when O_2 concentration approaches or exceeds the air-saturated value (Costache et al., 2013; Ippoliti et al., 2016; Sanchez Zurano et al., 2021).

In addition to the regulation by light intensity, water height and concentrations of O_2 and ODU, the process rates are additionally regulated by ambient temperature. In the present model, the temperature response is assumed to follow an empirical cardinal function, which captures an increase in rates at moderate temperatures and a catastrophic decline at supra-optimal temperatures (Bernard and Rémond, 2012; Ippoliti et al., 2016; Sanchez Zurano et al., 2021). Formally, it is implemented by expressing the rate coefficients of the modeled processes (i.e., photosynthesis, basal respiration, or reoxidation) as a product

$$r_j = r_{j,opt} \cdot \lambda_j(T), \tag{13}$$

where $r_{j,opt}$ is the optimal (i.e., maximal) value of the rate coefficient, reached at the optimal temperature $T = T_{j,opt}$, and $\lambda_j(T)$ is the corresponding cardinal function, formulated between the lower boundary ($T_{j,min}$) and upper boundary ($T_{j,max}$) according to

$$\lambda_j(T) = \frac{(T - T_{j,max}) \cdot (T - T_{j,min})^2}{(T_{j,opt} - T_{j,min}) \cdot [(T_{j,opt} - T_{j,min}) \cdot (T - T_{j,opt}) - (T_{j,opt} - T_{j,max}) \cdot (T_{j,opt} + T_{j,min} - 2T)]} \tag{14}$$

and equal to zero elsewhere (Fig. **S3**). In this expression, all temperatures are expressed in °C, and the index j indicates that the parameters in Eqs. 13–14 are, in general, process-specific. Note that in contrast to the rate coefficients, the fractions $c_{aeromin}$ and $c_{photoresp}$ are assumed to be temperature independent in the model.

2.2.5 Model calibration

The model uses a total of 34 parameters to formally describe the boundary conditions and the regulation of biogeochemical processes by environmental conditions. Some of these parameters were constrained by direct laboratory measurements or based on published literature, while most parameters were estimated by fitting the model predictions to the measured data, adopting the following approach (see details in Table **S3** and Supplementary Methods, section "Model calibration steps"). For parameters whose variation among the replicate sediment cores was not expected, the aim was to find only one representative value across all replicate sediment cores. This included the rate coefficients $r_{photosyn}$, $r_{basalresp}$ and r_{reox}, the fractions $c_{aeromin}$ and $c_{photoresp}$, the P-I response parameters k_I and w, and the temperature response parameters $T_{j,opt}$, $T_{j,min}$ and $T_{j,max}$, because these parameters are assumed to represent the physiological response of the studied microbial community. In contrast, for parameters whose variation among the cores was expected because of the natural variability in the sampled sediment (e.g., the total active MPB biomass, B_{MPB}, or the ODU concentration at the lower boundary of the modeled domain, C_{ODU}^{deep}), their optimal values were found individually per core, such that measurements performed in that core during a particular experiment (PI, TR or IE) could be reproduced by the model as well as possible. Finally, parameters for which it was plausible that they

https://doi.org/10.5194/egusphere-2026-4452
Preprint. Discussion started: 28 July 2026

would change in response to the experimental condition varying during a particular experiment (e.g., the peak location and dispersion of the MPB biomass, μ and σ, varying in response to increasing incident irradiance or temperature), their optimal values were found individually per condition and core.

A different approach was used when constraining the light attenuation coefficient, k_{ext}. On the one hand, the exponential model (Eq. 7) adequately described the average vertical profile of scalar irradiance, yielding the value of $k_{ext} = 4.6\,\mathrm{mm}^{-1}$ (Fig. **S4**). On the other hand, individual light profiles varied greatly both among and within replicate cores, with the corresponding k_{ext} values ranging between 2.5–20 mm^{-1} (Fig. **S4**). Additionally, some profiles did not follow the exponential model at all. Because of this high variability, and the fact that the light and O_2 measurements were not done at the exact same locations, model parameters controlling light attenuation (k_{ext}) and O_2 production (μ, σ, k_I and w) along the exact same vertical profile could not be constrained independently. Instead, they were all constrained based on the measured depth profiles of O_2 production rates. More specifically, for a particular core replicate, k_{ext} was estimated from the maximum depth of detectable O_2 production, paying attention that the value fell within the range derived from the light microsensor measurements.

2.2.6 Model implementation

The model functions were implemented in Fortran to optimize computational speed. The functions were then compiled into a dynamically linked library (DLL) and integrated with the R programming environment (R Core Team, 2023). The model is available as two distinct packages: `O2DIA` (Soetaert et al., 2025a), which provides a command line interface for model simulations, and `O2DIAshiny` (Soetaert et al., 2025b), which provides a graphical user interface. The finite-difference grid setup is facilitated by the R package `ReacTran` (Soetaert and Meysman, 2012), while the chemical and physical constants are calculated by the R package `marelac` (Soetaert et al., 2010a). The steady-state and dynamic solutions of the model are numerically solved using the R packages `rootSolve` (Soetaert, 2023) and `deSolve` (Soetaert et al., 2010b), respectively.

3 Results

3.1 O_2 measurements under different treatments

In the PI experiment, conducted at a constant temperature of 23 °C, an increase in the incident irradiance led to greater light availability within the MPB biofilm, yielding higher rates of photosynthetic O_2 production and thus greater O_2 concentrations in the upper few millimeters of the sediment (data-points in Fig. 1a–c). These trends are similar to those previously observed in comparable systems (Revsbech and Jørgensen, 1983; Al-Najjar et al., 2012; Haro et al., 2019b). Relatively large differences were observed among the replicate cores, in particular regarding the thickness of the photosynthetically active zone, O_2 penetration, and magnitude of O_2 concentrations at comparable illumination. O_2 production was typically detectable in the top 0.5 mm of the sediment at the lower levels of indicent light, with additional contributions from deeper layers (0.5–1 mm) as the incident light progressively increased.

https://doi.org/10.5194/egusphere-2026-4452
Preprint. Discussion started: 28 July 2026

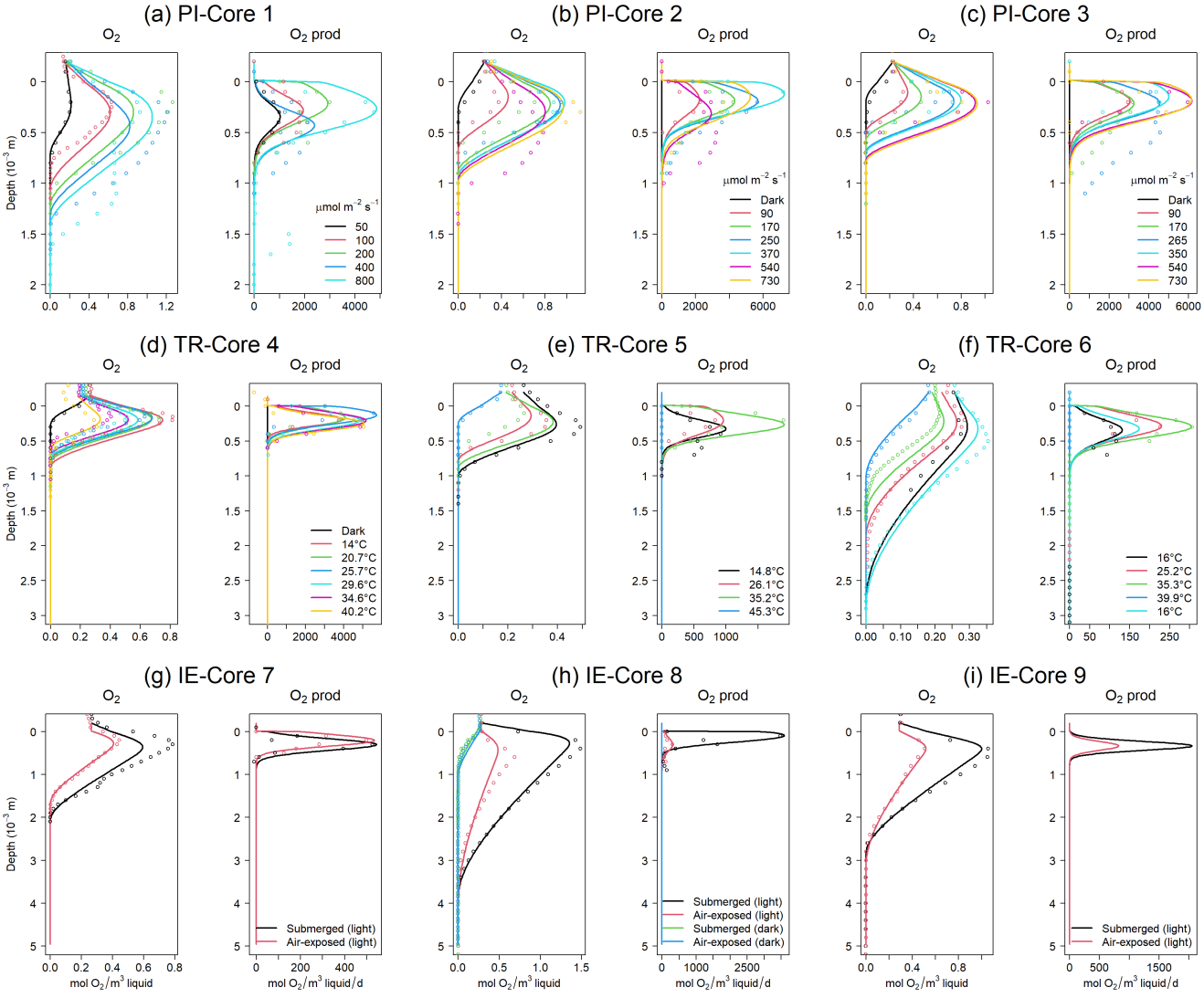

Figure 1. Vertical profiles of steady-state O_2 concentrations and gross rates of O_2 production in the studied MPB biofilms. Rows correspond to different experiments, while columns correspond to replicate sediment cores. (a–c) The photosynthesis–irradiance (PI) experiment in cores 1–3, (d–f) the temperature ramping (TR) experiment in cores 4–6, and (g–i) the immersion–emersion (IE) experiment in cores 7–9. In each panel, data points show measured data, lines depict predictions by a calibrated model, and colors differentiate among experimental conditions within each experiment, as specified in the legends and Table **S1**. Measured gross O_2 production data were not available for panel (i) because gross O_2 production could not be reliably quantified from the corresponding microsensor measurements.

https://doi.org/10.5194/egusphere-2026-4452
Preprint. Discussion started: 28 July 2026

However, we sometimes detected values that were inconsistent with this general pattern, such as the high O_2 production rates at depths 1.5–1.7 mm in core 1 (Fig. 1a) or the elevated rates in cores 2 and 3 in the depth range of 0.5–1 mm at incident light levels of 540 and 265 µmol photons/m^2/s, respectively (Fig. 1b,c). These observations are likely experimental artifacts caused by the displacement of MPB biomass by O_2 bubbles forming within the biofilm during the measurements. Such bubbles can form when the biological and chemical O_2 consumption combined with the diffusive transport are insufficient to counteract the extremely high photosynthetic O_2 production, leading to a local O_2 accumulation to super-saturated levels.

In the TR experiment, conducted at two levels of incident irradiance (150 and 320 µmol photons/m^2/s), rates of O_2 production progressively increased as the temperature increased from 14–16 °C until about 35 °C, whereas the steady-state O_2 concentrations declined (Fig. 1d–f). When temperature reached about 40 °C, O_2 production was still detectable in core 4 but collapsed to zero in core 6. Similar collapse in O_2 production occurred in core 5, but at 45 °C. In the absence of detectable O_2 production, O_2 concentration profiles resembled those measured under dark conditions in the PI experiment (Fig. 1e–f). Similar to the PI experiment, large inter-core variability was observed in the TR experiment, in particular with core 6 (Fig. 1f) showing much lower rates of gross O_2 production (roughly 10-fold) and somewhat deeper O_2 penetration and lower O_2 concentrations than the other replicate cores, including those from the PI experiment.

In addition to the detrimental effect of the most extreme thermal stress tested, a relatively rapid recovery of MPB photosynthesis was observed after the thermal stress was relieved. More specifically, in the replicate core 6 of the TR experiment, the gross O_2 production completely ceased at 40 °C, but recovered roughly to the same level 2 hours after the temperature was reduced back to the initial value of 16 °C (Fig. 1f). This recovery was also reflected in the profile of O_2 concentrations, which reached similar levels (even slightly higher) after the recovery than during the initial measurement at the same temperature (Fig. 1e).

In the IE experiment, conducted at the lower end of temperatures (10–15 °C) and intermediate levels of incident irradiance (150–230 µmol photons/m^2/s), air exposure of the sediment surface led to a pronounced decrease in O_2 concentrations compared with the submerged sediment (Fig. 1g–i). While this response was reproducible among the three core replicates, the response of the O_2 production rates varied greatly: while core 7 showed barely any change both in the vertical distribution and magnitude of the rates between the two conditions (Fig. 1g), sediment emersion in core 8 led to a drop in O_2 production to less than 5 % of the rates observed in the submerged sediment. No O_2 production rates were measured in core 9.

3.2 Model calibration

Overall, model calibration based on the present experimental data was challenging, primarily due to the large differences among the replicate sediment cores but also because of the impact of likely experimental artifacts on data quality (see above). Nevertheless, although noticeable deviations remain, the calibrated model captured reasonably well the general patterns and trends observed (compare data-points and lines in Fig. 1).

Best estimates of the parameters $r_{photosyn}$, $r_{basalresp}$, $c_{aeromin}$, $c_{photoresp}$, k_I, w and m were the same or very similar among the replicate cores (Table 1), consistent with the assumption that they represent intrinsic properties of the microbial

https://doi.org/10.5194/egusphere-2026-4452
Preprint. Discussion started: 28 July 2026

Table 1. Best estimates of the model parameters. Values were constrained based on the experimental data and are shown separately for each replicate core. Averages from cores 1–3 were used in Monte-Carlo (MC) simulations.

Parameter	Experiment									MC simulations
	PI			TR			IE			
	Core 1	Core 2	Core 3	Core 4	Core 5	Core 6	Core 7	Core 8	Core 9	
T (°C)[§]	23	22.5	23	–	–	–	15	14.8	10	23
C_{MPB} ($\mathrm{mol\,C/m^2}$)	27	18	27	14.4	7.2	4.32	3.78	7.2	7.2	24[†]
μ (mm)[♯]	0.40–0.65	0.12–0.50	0.27–0.44	0.15–0.29	0.27–0.40	0.62–0.70	0.29–0.46	0.11–0.55	0.40	0.39
σ (mm)[♯]	0.16–0.40	0.21–0.36	0.12–0.35	0.09–0.15	0.15–0.40	0.25–0.30	0.18	0.18–0.25	0.12	Eq. 15
$r_{photosyn}$ ($\mathrm{d^{-1}}$)	0.15	0.15	0.15	0.15	0.15	0.15	0.15	0.15	0.15	0.15
$r_{basalresp}$ ($\mathrm{d^{-1}}$)	0.0002	0.0002	0.0002	0.008	0.002	0.0002	0.0002	0.0002	0.0002	0.0002
r_{reox} (dark) ($\mathrm{d^{-1}}$)	–	1000	1000	–	–	–	–	–	–	1000
r_{reox} (light) ($\mathrm{d^{-1}}$)	5000	5000	5000	7500	5000	500	1000	1000	300	5000
c_{min}	0.35	0.4	0.4	0.4	0.4	0.2	0.01	0.01	0.4	0.38
$c_{photoresp}$	0.001	0.001	0.001	0.001	0.001	0.001	0.001	0.001	0.001	0.001
k_I ($\mathrm{\mu mol\,photons/m^2/s}$)	150	150	300	150	150	150	150	150	150	200[†]
w	10	10	10	10	10	10	10	10	10	10
m	4	4	4	4	4	4	4	4	4	4
C_{ODU}^{deep} ($\mathrm{mol\,O_2/m^3 liquid}$)	7	12	20	11	6	2	2	2	2	13[†]
g_0	–	–	–	–	–	–	0.5	0.4	0.4	0.4[†]
$T_{prod,max}$ (°C)	–	–	–	45	45	40	–	–	–	43.3
$T_{prod,min}$ (°C)	–	–	–	−20	−20	−50	–	–	–	−30
$T_{prod,opt}$ (°C)	–	–	–	36	36	34	–	–	–	35.3
$T_{reox,max}$ (°C)	–	–	–	55	55	55	–	–	–	55
$T_{reox,min}$ (°C)	–	–	–	−10	−10	10	–	–	–	−3.3
$T_{reox,opt}$ (°C)	–	–	–	45	45	45	–	–	–	45
$T_{basalresp,max}$ (°C)	–	–	–	48	48	48	–	–	–	48
$T_{basalresp,min}$ (°C)	–	–	–	10	10	10	–	–	–	10
$T_{basalresp,opt}$ (°C)	–	–	–	35	35	35	–	–	–	35

[§]Experimental temperature, measured directly. [♯]The range of values for parameters μ and σ is shown in Fig. **S5**. [†]In MC simulations, this value was additionally varied uniformly by ±10%. For g_0, this variation was only applied for the IE forcing scenario.

https://doi.org/10.5194/egusphere-2026-4452
Preprint. Discussion started: 28 July 2026

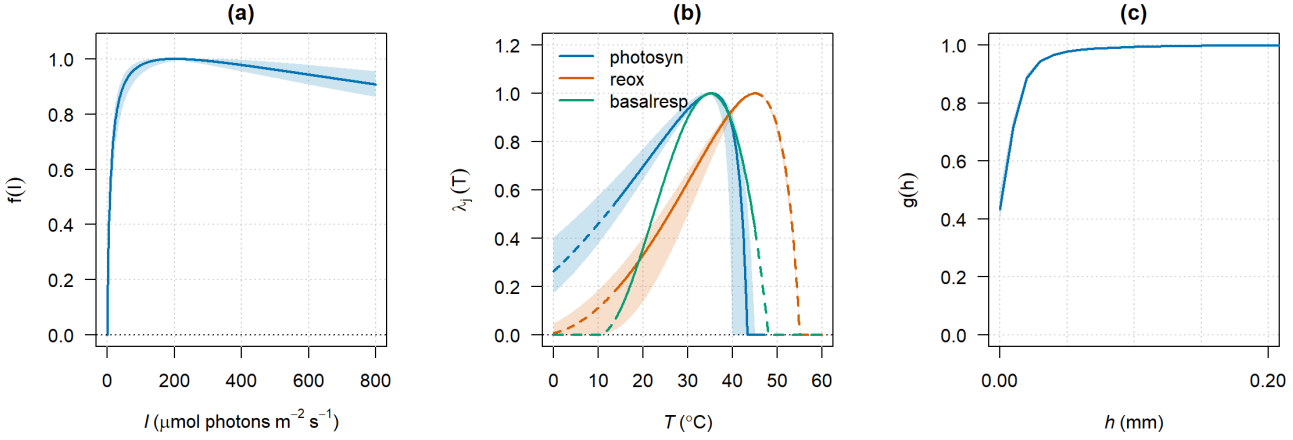

Figure 2. Estimates of functions describing the response of specific processes in the studied sediments to changes in environmental conditions. (a) Light response of MPB photosynthesis (Eq. 6). I corresponds to the intensity of light to which MPB cells at a particular depth in the sediment are exposed. (b) Temperature response of MPB photosynthesis, ODU reoxidation, and MPB basal respiration (Eq. 14). Solid lines correspond to the range covered in our experiments, dashed lines incidate predictions by the cardinal function outside of this range. (c) Response of MPB photosynthesis to sediment emersion (Eq. 8). h denotes the water height above the sediment surface. In all panels, solid lines depict the best estimates, shaded areas represent the minimum–maximum envelope derived based on data from 3 replicate cores.

community driving the modeled processes. The estimated values of $k_I = 150\,\mu\text{mol photons}/\text{m}^2/\text{s}$ and $w = 10$ indicate that photosynthesis is very efficient at low light levels and only slightly impacted by photoinhibition at very high light levels (see the corresponding light response curve in Fig. 2a).

In contrast, parameters B_{MPB} and C^{deep}_{ODU} varied considerably among the replicate cores (Table 1), reflecting the natural variability of the studied sediments. The estimated range of B_{MPB} (3.8–27 $\text{mol C}/\text{m}^2$) was consistent with the large intra- and inter-core variability determined for the Chl *a* content in the surface sediment layer (3.2–34.8 $\text{mol C}/\text{m}^2$; Table **S2**). Although these two quantities are related, constraining B_{MPB} for each core directly from the corresponding Chl *a* content was not possible because of the different spatial scales at which these two quantities were determined ($<\text{mm}^2$ for B_{MPB} versus cm^2 for Chl *a*). Regarding the parameter C^{deep}_{ODU}, which represents concentrations of reduced porewater solutes such as ammonia or dissolved sulfide or iron in deeper sediment layers, its estimated inter-core variability (by a factor of 10; Table 1) is plausible but could not be verified due to the lack of direct measurements of these substances.

When analysing the data from the PI experiment, we found that they could not be consistently reproduced by the model unless MPB biomass was allowed to vertically redistribute in response to the variation in incident irradiance. More specifically, we found that the parameter σ, which describes the vertical dispersion of the MPB distribution (Eq. 4), systematically increased with increasing incident irradiance (Fig. **S5**a). This pattern was reproducible among the replicate cores and could be approximated by a linear relationship,

$$\sigma(I_a) \approx 0.2 \times 10^{-3} + 2.25 \times 10^{-7} \cdot I_a, \tag{15}$$

https://doi.org/10.5194/egusphere-2026-4452
Preprint. Discussion started: 28 July 2026

where the incident irradiance, I_a, is in $\mu\mathrm{mol\,photons/m^2/s}$. In contrast, the parameter μ, which describes the depth of maximal MPB biomass concentration, showed modest differences among the cores but no systematic relationship with the incident irradiance (Fig. **S5**a). Overall, these findings suggest that light availability controls O_2 dynamics in the sediments not only directly by affecting MPB photosynthesis, but also indirectly by inducing MPB redistribution within the surficial sediment.

Another notable pattern identified when fitting the data from the PI experiment was that the parameter r_{reox}, which describes ODU reoxidation, needed to increase by a factor of 5 between the dark and light conditions (Table 1). Because the O_2 penetration depth markedly differs between these two conditions (Fig. 1a–d), this finding suggests significant differences in ODU reoxidation depending on whether it occurs closer to the sediment interface (at depths $z \lesssim 0.25\,\mathrm{mm}$) or at greater depths ($z \gtrsim 0.5\,\mathrm{mm}$).

When fitting the data from the TR experiment, we found that parameters $c_{aeromin}$ and $c_{photoresp}$ remained unchanged across the different temperatures tested and were consistent among replicate cores (Table 1). In contrast, the rate coefficients $r_{photosyn}$, $r_{basalresp}$ and r_{reox} showed temperature dependency which was adequately described by the cardinal function (Fig. 2b). More specifically, photosynthetic O_2 production increased steadily with rising temperature, peaking at around $35\,^\circ\mathrm{C}$ before sharply declining to zero at 40–$45\,^\circ\mathrm{C}$. Basal respiration followed a similar trend but increased more steeply at lower temperatures than O_2 production, whereas ODU reoxidation showed greater thermal tolerance than O_2 production, peaking at around $45\,^\circ\mathrm{C}$. Our modeling analysis suggested that ODU reoxidation would decline to zero at about $55\,^\circ\mathrm{C}$, but the range of temperatures tested in this study was insufficient to verify this. Additionally, we found that only minor modifications of the parameters describing the vertical MPB biomass distribution (μ and σ) were necessary when fitting the data from the TR experiment (Fig. **S5**b). Overall, these findings suggest that temperature controls O_2 dynamics in the sediments by directly, but differently, affecting the O_2 producing and consuming processes.

When analysing the data from the IE experiment, we could reproduce the data by assuming that the photosynthetic O_2 production decreased by a factor of 0.4–0.5 when the sediment surface became exposed to air (Fig. 2c). Although the changes in O_2 production observed in the replicate core 8 additionally suggested downward migration of MPB in response to sediment emersion, this response was not supported by data collected in the replicate core 7 (cf. Fig. 1g and 1h).

3.3 Model output

The model generates vertical profiles of the two state variables and process rates as a function of time, together with the corresponding average and maximum O_2 concentrations in the oxic zone, O_2 penetration depth, depth-integrated process rates, and O_2 and ODU fluxes across the model boundaries. This output enables comprehensive evaluation of how O_2 production, internal recycling and exchange with the overlying water impact O_2 availability and budgets in the sediment. To illustrate this under steady state conditions, we visualize the model output for a system with representative properties and under a range of environmental conditions. The choice of the representative properties was guided by the range of values estimated for the replicate cores from the PI experiment (Table 1), including the empirical trend identified for σ (Eq. 15), while the range of environmental conditions aligned with those used in our experiments. Because of the model's sensitivity to the parameter values, in particular to C_{MPB}, C_{ODU}^{deep}, $k_{\mathrm{ext,solid}}$ and θ, we emphasize that the results presented below should be treated as

https://doi.org/10.5194/egusphere-2026-4452
Preprint. Discussion started: 28 July 2026

illustrative examples of the trends and patterns in the response of a particular system to specific variations in environmental forcing.

3.3.1 Vertical distribution of model variables and process rates

In the PI forcing scenario, increasing incident irradiance at the SWI increases light availability inside the sediment, broadens the MPB biomass distribution, and shifts photosynthetic O_2 production slightly deeper into the sediment (Fig. 3a). In the dark and at low irradiance levels, O_2 consumption has a single dominant peak, mainly associated with ODU reoxidation near the lower edge of the oxic zone. With increasing irradiance, enhanced O_2 production raises O_2 concentrations and deepens O_2 penetration, and the consumption profile develops a distinct bimodal structure: a near-surface peak linked to MPB-associated aerobic mineralization and respiration, and a deeper peak caused by ODU reoxidation. These two O_2 consumption peaks show different sensitivity towards light. While the surface peak increases substantially in magnitude and spreads slightly towards deeper layers as the incident irradiance increases, the deeper peak mostly shifts downward, with only a modest increase in the vertical spread and magnitude. As a direct consequence of this spatial reorganization, ODU is progressively depleted from the surface layer, and the depth at which ODU starts to accumulate shifts downward.

In the TR forcing scenario, incident irradiance is fixed and so the light field and MPB biomass distribution remain unchanged while process rates respond to temperature (Fig. 3b). At sufficiently strong levels of incident irradiance, low temperatures yield the bimodal structure of the O_2 consumption processes described above, with a surface component linked to MPB production and a deeper component associated with ODU reoxidation. As temperature increases, O_2 production and O_2 consumption first increase, but a stronger increase in consumption reduces O_2 concentrations and penetration, causing the consumption zone and the ODU reoxidation peak to shift upward. At temperatures exceeding the photosynthetic optimum (and close to the optimum for ODU reoxidation), O_2 production rapidly declines and the O_2 consumption profile changes from a bimodal structure to a single near-surface peak resembling the dark state.

In the IE forcing scenario, the effects of sediment emersion are much more pronounced under light compared to dark conditions (Fig. 3c). Under light conditions, air exposure reduces O_2 production by the dry-production factor (about 0.4). In combination with the reduction in the DBL thickness to zero and the sustained supply of ODU from deeper sediment layers, this leads to substantially lower O_2 concentrations, shallower O_2 penetration, and reduced O_2 consumption confined to a narrower zone closer to the sediment surface. In the dark, DBL reduction under air exposure leads to a slightly stronger surface O_2 supply due to atmospheric exchange, causing a slight increase in O_2 penetration and thus broadening of the ODU reoxidation zone.

3.4 O_2 budgets and availability

In the PI forcing scenario, the depth-integrated gross O_2 production increases with incident irradiance and approaches a plateau of approximately $1.4\,\mathrm{mol\,O_2/m^2/d}$ at the highest irradiance levels (Fig. 4a). The sediment acts as a net O_2 sink in the dark, with the corresponding O_2 flux at the SWI of $0.1\,\mathrm{mol\,O_2/m^2/d}$, and shifts to a net O_2 source as the incident irradiance increases above the compensation irradiance of $\sim 30\,\mu\mathrm{mol\,photons/m^2/s}$. At all irradiance levels, most of the O_2 produced by

https://doi.org/10.5194/egusphere-2026-4452
Preprint. Discussion started: 28 July 2026

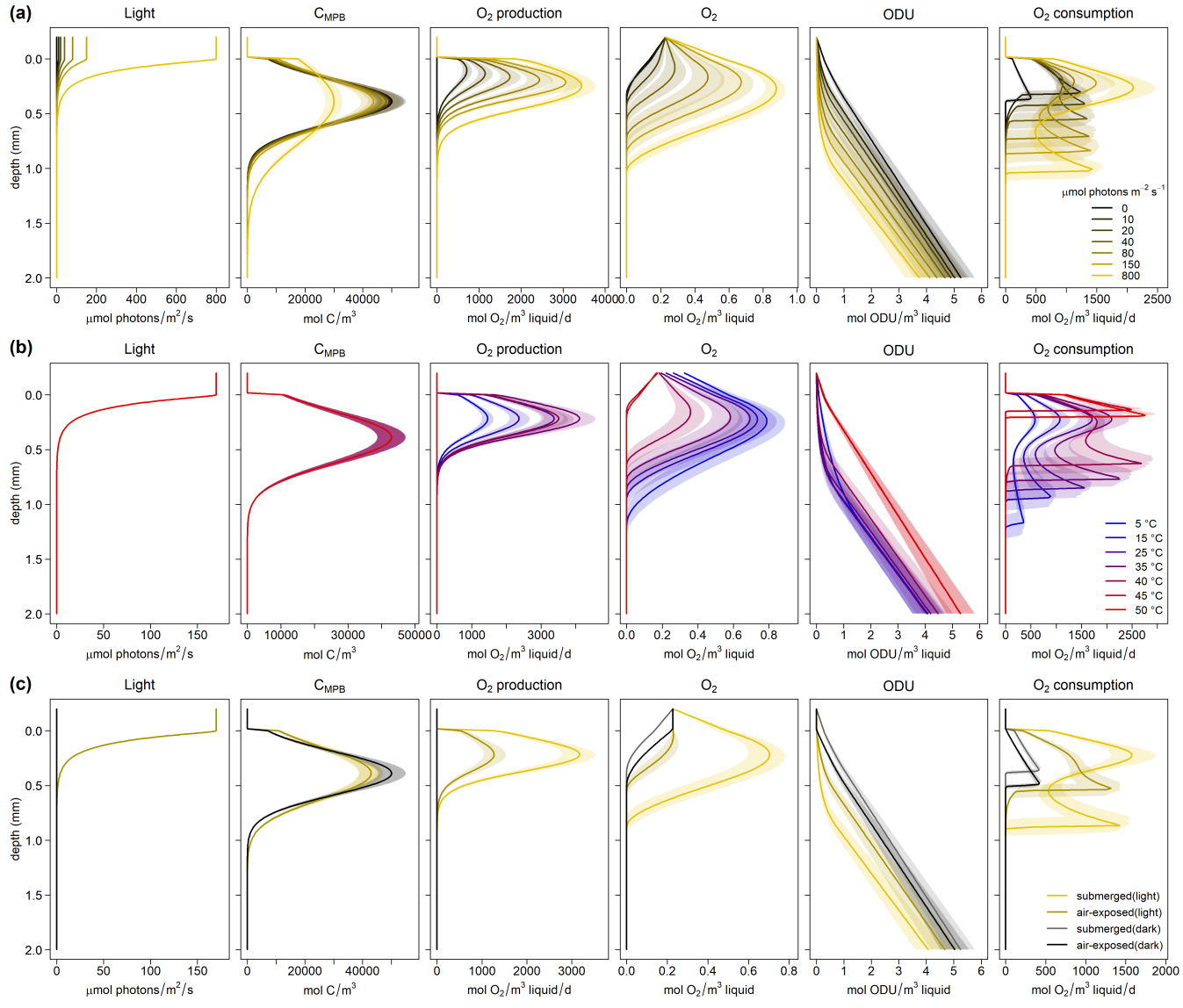

Figure 3. Examples of an output generated by the O2DIA model. Shown are steady-state vertical profiles of light, MPB biomass, O_2 production, O_2 concentration, ODU concentration, and total O_2 consumption in response to varying (a) incident irradiance, (b) ambient temperature, and (c) sediment emersion. Solid lines show the output for a system with representative properties (shown in Table 1, column "MC simulations"), shaded bands show the min–max envelope from 100 Monte Carlo simulations in which selected parameters were varied uniformly within $\pm 10\,\%$ of their representative values. Different forcing conditions are depicted in different colors, as indicated in the legends.

https://doi.org/10.5194/egusphere-2026-4452
Preprint. Discussion started: 28 July 2026

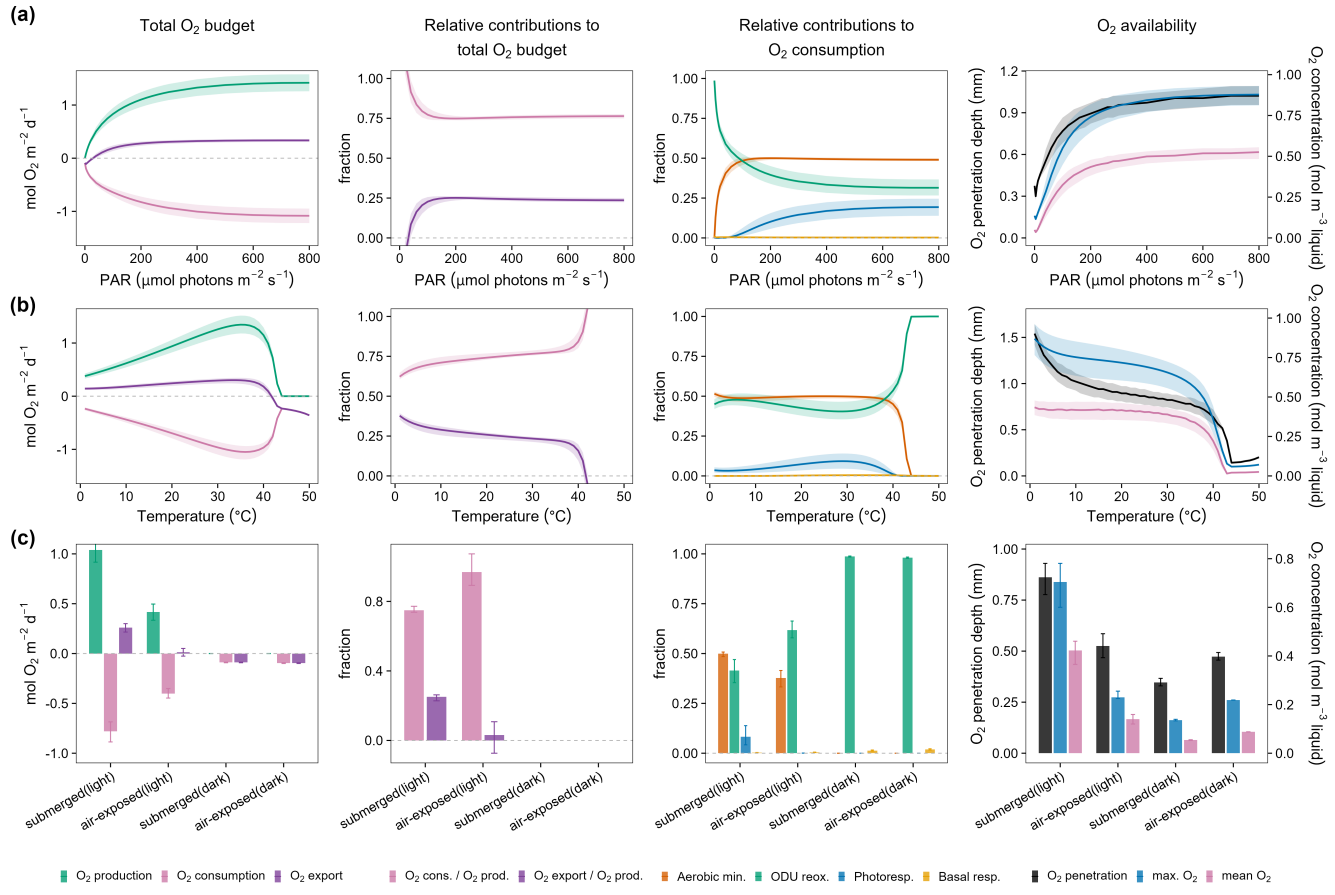

Figure 4. Examples of an output generated by the O2DIA model. Shown are various metrics describing O_2 budgets and availability in the sediment under steady-state conditions in response to varying (a) incident irradiance, (b) ambient temperature, and (c) sediment emersion. The first column shows the depth-integrated rates of O_2 production by MPB photosynthesis, total O_2 consumption, and the corresponding net O_2 flux at the sediment surface (positive values represent net export into the overlying water or air, negative values represent net import into the sediment). The second column shows total O_2 consumption and O_2 export normalized to O_2 production, representing the relative degrees of internal O_2 recycling and net autotrophy within the system, respectively. The third column shows relative contributions of aerobic mineralization, ODU reoxidation, photorespiration, and basal respiration to total O_2 consumption. The fourth column shows O_2 penetration depth into the sediment (left axis) and the maximum and mean O_2 concentration within the oxic zone of the sediment (right axis). Simulations were performed for ambient temperature of 23 °C (panels a and c) and incident irradiance of 170 $\mu mol photons/m^2/s$ (panels b and c). Solid lines and bars show the output for a system with representative properties (shown in Table 1, column "MC simulations"), shaded bands and error-bars show the min–max envelope from 100 Monte Carlo simulations in which selected parameters were varied uniformly within ±10 % of their representative values.

https://doi.org/10.5194/egusphere-2026-4452
Preprint. Discussion started: 28 July 2026

MPB photosynthesis is internally recycled by the O_2 consuming processes. For example, O_2 recycling decreases from $100\,\%$ reached at the compensation point and stabilizes at about $75\,\%$ at intermediate to high irradiance levels. Consequently, O_2 export into the overlying water does not exceed $25\,\%$ from production. ODU reoxidation is by far the most dominant pathway of O_2 consumption at low irradiance levels. However, as the irradiance increases, this dominant role is sharply overtaken by aerobic mineralization, whose relative contribution stabilizes at about $50\,\%$ at intermediate to high irradiance levels. In this range, the contribution of photorespiration also becomes progressively more significant, reaching about $20\,\%$ at the highest irradiance levels. Basal respiration remains a minor component of the total O_2 consumption throughout, contributing less than $1.3\,\%$.

This light-dependent balance between the O_2 producing and consuming processes directly impacts O_2 availability in the sediment (Fig. 4a). For example, O_2 penetration increases from about $0.37\,\mathrm{mm}$ in the dark until about $1\,\mathrm{mm}$ at the highest irradiance levels, and this increase is accompanied by a gradual raise in the average and maximum O_2 concentrations within the oxic zone, which reach up to 0.53 and $0.88\,\mathrm{mol\,O_2/m^3_{liquid}}$, respectively.

In the TR forcing scenario, depth-integrated gross O_2 production increases with temperature, reaching a peak of $\sim 1.3\,\mathrm{mol\,O_2/m^2/d}$ at $35\,^\circ\mathrm{C}$ before declining sharply towards zero at higher temperatures (Fig. 4b). O_2 consumption shows a similar pattern but remains significant over a broader high-temperature range because of the greater thermal tolerance of ODU reoxidation compared to photosynthesis. In the temperature range between 1–$38\,^\circ\mathrm{C}$, the level of internal O_2 recycling gradually increases from $62\,\%$ to $80\,\%$. Thus, in this temperature range, the sediment's degree of net autotrophy declines from $38\,\%$ to $20\,\%$. Aerobic mineralization contributes roughly $50\,\%$ to the total O_2 consumption in this temperature range, while ODU reoxidation combined with photorespiration contribute the remaining $50\,\%$. Once O_2 production starts collapsing at temperatures above $42\,^\circ\mathrm{C}$, the sediment shifts from a net O_2 source to a net O_2 sink, with ODU reoxidation being the main pathway of O_2 consumption. Similar to the PI scenario, the contribution of basal respiration remains negligible at all temperatures.

As a result of this temperature-dependent balance between the O_2 producing and consuming processes, O_2 penetration gradually declines from $1.5\,\mathrm{mm}$ to $0.7\,\mathrm{mm}$ in the temperature range between 1–$38\,^\circ\mathrm{C}$, followed by a sharp drop towards $\sim 0.2\,\mathrm{mm}$ above $43\,^\circ\mathrm{C}$ due to the collapse of photosynthesis combined with a stronger temperature tolerance of ODU reoxidation (Fig. 4b). This declining trend is accompanied by a similar pattern for the average and maximum O_2 concentrations within the oxic zone.

In the IE forcing scenario, the most notable effect occurs under light conditions, where O_2 export across the sediment surface drops from $\sim 0.26\,\mathrm{mol\,O_2/m^2/d}$ under submerged conditions to near-zero under air exposure (Fig. 4c). This drop is driven by the contrasting responses of O_2 production and ODU reoxidation to sediment emersion: while the former drops by $\sim 60\,\%$, the latter remains persistently strong under both submerged and air-exposed conditions. This large drop is also accompanied by the correspondingly large reductions in O_2 penetration and maximum and average O_2 concentrations in the oxic zone. In the dark, the effects of sediment emersion on O_2 availability and budgets are reversed, albeit relatively minor. The DBL compression associated with air exposure increases the O_2 flux into the sediment by $\sim 8\,\%$, leading to a slightly deeper O_2 penetration and higher maximum and average O_2 concentrations. The O_2 consumption is almost fully driven by ODU reoxidation.

https://doi.org/10.5194/egusphere-2026-4452
Preprint. Discussion started: 28 July 2026

4 Discussion

The model developed in the present study provides new insights into the mechanisms governing O_2 dynamics in MPB-inhabited intertidal sediments. Interpretation of the model results, however, requires careful consideration of the key model assumptions and uncertainties. In the following sections, we first discuss these assumptions and uncertainties before examining the specific implications of the model for MPB migration and oxygen production and consumption in the studied system, including their response to light, warming and tidal forcing. Finally, we assess the broader applicability of the model and identify points of further improvement.

4.1 Model assumptions and uncertainties

An important assumption in the present model is that the total active MPB biomass in the surface sediment layer is imposed and remains constant through the experiments. Although we did estimate MPB biomass via Chl-*a* measurements in samples collected from the experimental cores, these measurements showed substantial variability or were sometimes unreliable due to the limited amount of MPB biomass (Table **S2**). Additionally, the conversion from Chl-*a* to carbon biomass carries a large level of uncertainty (Geider et al., 1997), and surface Chl-*a* samples may not fully represent the metabolically active MPB biomass in the sediment. Thus, we used the Chl-*a* measurements only to constrain the order of magnitude of the active MPB biomass while treating this quantity as an adjustable parameter in the model to explain the variability among the experimental cores. This approach allowed us to use the same value for the rate coefficient $r_{photosyn}$ (which represents the gross photosynthetic O_2 production rate normalized per unit of MPB biomass) across all replicate cores, consistent with the assumption that this parameter represents an intrinsic physiological property of the studied MPB community.

An important uncertainty in the present model involves parameters that characterize the photosynthesis–irradiance response of the studied MPB community (k_I and w), caused by highly variable and sometimes inconsistent measurements of light attenuation in the sediment. In line with previous studies, we modeled light attenuation in the sediment using an exponentially decreasing function of depth, parameterized by the light extinction coefficient k_{ext}. However, our measurements with a scalar irradiance microprobe sometimes deviated from this idealized model and showed great variability even if measured in locations only a few millimeters apart. These findings showed that the studied MPB biofilms were horizontally and vertically highly heterogeneous, at least with respect to the MPB biomass concentration, and additionally indicated that the simple exponential function, although adequate on average (Fig. **S4**), may not be an adequate model of light attenuation for any particular horizontal location.

Because we did not perform O_2 and light measurements at the exact same locations, the high results variability implied that we could not directly link the rate of photosynthetic O_2 production at a particular depth in the sediment with an accurately measured value of the locally available light. Instead, we linked the O_2 production rate with a light level that was calculated based on the assumption that light attenuates exponentially with depth and penetrates as far as the maximum depth of detectable O_2 production.

https://doi.org/10.5194/egusphere-2026-4452
Preprint. Discussion started: 28 July 2026

Based on this approach, our results indicate that photosynthesis by the studied MPB community is very efficient at low light levels and only slightly impacted by photoinhibition at very high light levels (Fig. 2a). We emphasize, however, that because we used an indirect approach to constrain the parameters k_I and w, their estimates may be inaccurate, with an unknown degree of uncertainty. To overcome this issue, future studies need to conduct parallel O_2 and light microsensor measurements in locations that are not more than $\sim 100\,\mu m$ apart or use a different, more direct experimental approach to evaluate the community's light response.

4.2 Simplified representation of MPB migration

Light is regarded as one of the main drivers of MPB vertical migration (Haro et al., 2019a). Additionally, it directly affects the functioning of their photosynthetic apparatus, triggering photoprotective mechanisms and causing photoinhibition (Serôdio et al., 2005). An earlier study on the migratory photoresponse of MPB showed a clear biphasic pattern: as the incident irradiance increased from low to high levels, MPB biomass in the upper sediment layer increased at low levels, reached a maximum at intermediate levels, and subsequently declined at higher levels due to a photophobic downward migration of cells away from the sediment surface (Serôdio et al., 2006).

In the present study, the vertical MPB biomass distribution is described by two parameters, σ and μ, reflecting a simplified, empirical-based parameterization rather than a mechanistic representation of the underlying process. Our analysis suggested that the parameter σ, which describes the vertical spread of the biomass distribution, increased with irradiance level (Fig. **S5**, Eq. 15), indicating that the biomass distribution extended deeper into the sediment with increasing irradiance. Although the estimated values of μ, which describes the depth of the peak MPB biomass, varied considerably among irradiance levels and replicate cores, they showed a slight decrease with increasing irradiance. However, this trend was not statistically significant ($p = 0.357$). Thus, our results support a light-induced broadening of the vertical biomass distribution but not a systematic downward shift of the biomass maximum. In contrast, Haro et al. (2019b) reported an initial upward migration under low to intermediate irradiance, followed by a downward migration at higher irradiance. One possible explanation for this difference is the much stronger light attenuation in our sediment system compared with the biofilm system investigated by Haro et al. (2019b). Because of this stronger light attenuation, MPB residing in deeper sediment layers likely remained light-limited across the entire range of irradiance applied in our experiments. Increasing the incident irradiance therefore allowed photosynthetically favorable conditions to extend to greater sediment depths, leading to a broader vertical distribution of the active biomass, but the light available at depth apparently did not reach sufficiently high levels to induce photoprotection-driven downward migration for the majority of the MPB community, which would manifest as a measurable downward shift in the position of the biomass maximum.

4.3 New quantitative constraints on reoxidation and photorespiration

O_2 in intertidal sediments is known to be primarily consumed via (i) aerobic heterotrophic activity of fauna and bacteria and (ii) reoxidation of reduced inorganic compounds released during anaerobic organic matter mineralization. However, a direct method to measure the relative importance of these pathways remains elusive (Glud, 2008). In the present study, we

https://doi.org/10.5194/egusphere-2026-4452
Preprint. Discussion started: 28 July 2026

measured both O_2 production rates and steady-state vertical O_2 profiles that result from the combined effects of production and consumption. By explicitly formulating the total O_2 consumption as a sum of multiple pathways, each described by a mechanistic-like rate expression, the model allowed us to separately estimate their individual impacts and contributions.

Using this approach, we found that O_2 consumption via reoxidation of reduced compounds primarily controls the O_2 penetration depth, whereas basal respiration, aerobic mineralization, and photorespiration mainly act to reduce O_2 concentrations in the oxic zone of the sediment, i.e., where MPB photosynthesis is detectable. Basal respiration occurs both in the light and in the dark, but its contribution to total O_2 consumption remains small. In contrast, aerobic mineralization and photorespiration are indirectly coupled to light through O_2 production and thus mainly contribute under illuminated conditions. Aerobic mineralization increased rapidly with irradiance and accounted for approximately 30–50% of total O_2 consumption under moderate to high light, whereas photorespiration was negligible at low irradiance but increased to $\sim$20% at the highest irradiance levels. Taken together, these processes shape O_2 dynamics in intertidal sediments by jointly regulating both the penetration depth and concentrations of O_2 near the sediment surface.

During model calibration, it was necessary to treat ODU reoxidation under light and dark conditions differently. More specifically, we needed to use a larger reoxidation rate coefficient (r_{reox}) under light conditions compared to the dark in order to adequately model the measured O_2 profiles. A possible explanation for this difference is that the measured O_2 profiles were still in a transient state, while the calibration assumed that a steady state was reached. This hypothesis is plausible because ODU are supplied from a much thicker sediment layer than the oxic zone, and thus the response of the ODU profile to changes in O_2 availability (caused by changes in illumination) is much slower than the response of the O_2 profile to changes in illumination. However, a true steady-state O_2 profile can only be reached if the ODU profile also reaches a steady state. It is possible that steady-state ODU and O_2 profiles were never truly reached during our PI experiments, because the intervals of steady, but progressively increasing, illumination were insufficiently long. Modeling tests based on dynamic simulations rather than steady-state solutions are required to evaluate whether this effect alone can explain the apparent difference in r_{reox} between light and dark conditions.

Another plausible explanation could be the presence of solid-phase ODU, which are not included in the model. In sediments, reduced compounds may accumulate in deeper layers over longer timescales as solid-phase ODU (e.g., FeS; Canfield et al. (2005)), particularly in permanently anoxic layers or at depths where O_2 is present only under very strong illumination of the sediment surface, which may be rare under natural conditions. Hence, if such a strong illumination occurs, such as during our PI experiments, O_2 produced by MPB photosynthesis will reach these accumulated reduced pools, effectively increasing the local O_2 demand without requiring a change in the reaction rate coefficient. Another possibility is that, due to pH dependency of speciation of ODU constituents such as sulfide or ammonia (Canfield et al., 2005; Malkin and Meysman, 2015), ODU reoxidation is sensitive to variation in pH, which is known to occur in MPB biofilms as a result of rapid CO_2 uptake by photosynthesis in the light and net CO_2 release in the dark (Kühl et al., 1996). These hypotheses could be tested by conducting high spatial resolution ODU measurements and including the components and mechanisms mentioned above in the model.

In addition to aerobic heterotrophic activity and reoxidation, photorespiration is another pathway contributing to O_2 consumption in the sediment exposed to light. Previous studies showed that high photosynthesis rates in dense MPB communities

https://doi.org/10.5194/egusphere-2026-4452
Preprint. Discussion started: 28 July 2026

elevate pH and O_2 concentration while depleting CO_2, creating an oxidative environment with elevated reactive oxygen species (ROS), thereby inducing intensive photorespiration (Glud et al., 1992; Kühl et al., 1996). Photorespiration may account for carbon equivalents subsequently lost from gross photosynthesis measured with O_2 microsensors (Glud et al., 1992), yet the impact of this pathway has not been quantitatively constrained in natural biofilm systems.

In the present study, we formulated photorespiration as a fraction of O_2 production modulated by a power function of O_2 concentration (Eq. 10), in line with the empirical relationship proposed in industrial studies on microalgae cultivation (Costache et al., 2013). The value for the exponent estimated from the present data ($m = 4$; Table 1) aligned well with the previously reported values between 2.9 and 5 (Costache et al., 2013; Ippoliti et al., 2016). Using this relationship, we found that O_2 losses due to photorespiration were negligible at low light intensities but reached up to approximately 20% of the photosynthetically produced O_2 at high irradiance (Fig. 4a).

4.4 The impact of warming on O_2 production and consumption

The overall temperature response of a benthic ecosystem comprises contributions from multiple processes. Traditionally, this response is quantified through the parameter Q_{10}, which indicates the relative increase in the rate of a process when temperature increases by $10\,^{\circ}C$. Previous studies on diatom-covered sediments reported Q_{10} values of 2.2–2.6 for photosynthetic O_2 production and 2.6–5.6 for O_2 consumption by aerobic mineralization, indicating a tendency of the system to shift from net autotrophy towards net heterotrophy as the temperature increases (Hancke and Glud, 2004). However, the simple Q_{10}-based formulation cannot capture thermal inhibition at temperatures above the optimum.

To model the temperature response observed in the present study, in particular the collapse of O_2 production at high temperatures, we employed a cardinal function (Rosso et al., 1993; Bernard and Rémond, 2012), which begins with a gradual increase, peaks at an optimal temperature, and then sharply declines to zero at high, potentially damaging temperatures. This approach allowed us to reproduce the system's gradual shift towards a lower degree of net autotrophy with increasing temperature (Fig. 4b), consistent with previous observations by Hancke and Glud (2004). Additionally, using this approach we found that O_2 consumption had a higher optimal temperature and heat tolerance than photosynthesis (both by roughly $10\,^{\circ}C$), which aligns well with the results of earlier studies on single-species algae, where the optimal temperature for photosynthesis is typically around $35\,^{\circ}C$, while the maximum temperature is about $45\,^{\circ}C$ or even $50\,^{\circ}C$ (Costache et al., 2013; Ippoliti et al., 2016).

The mechanisms underlying the decline in productivity at high temperatures have been investigated extensively. Elevated temperatures can lead to protein denaturation, including critical enzymes involved in photosynthesis (Berry and Bjorkman, 1980). High temperatures may also disrupt the electron transport chain, particularly in photosystems PSII and PSI (Allakhverdiev et al., 2008), and cause an accumulation of ROS (Mittler, 2002; Apel and Hirt, 2004), leading to cellular damage, DNA mutations, and lipid peroxidation. In densely packed algal communities, increased temperatures can result in local pH imbalances, disrupting cellular functions (Giordano et al., 2005), and leading to the degradation of chlorophyll and other pigments vital for photosynthesis (Havaux, 1993).

In the final replicate of the temperature ramping experiment, we observed a complete cessation of O_2 production at $40\,^{\circ}C$, followed by a full recovery about $2\,h$ after the temperature was reduced back to the baseline value of $16\,^{\circ}C$. This finding

https://doi.org/10.5194/egusphere-2026-4452
Preprint. Discussion started: 28 July 2026

suggests that, in the studied MPB community, mechanisms such as enzyme function restoration, repair of photodamage to PSII, and ROS reduction enable a relatively fast recovery of photosynthetic productivity from high-temperature stress. It also suggests that, on the time scales of hours and at temperatures up to 40–45 °C, models utilizing the cardinal function to describe the temperature response of MPB photosynthesis may assume that the response is instantaneous and reversible.

4.5 Impact of sediment emersion on O_2 dynamics

Our measurements showed consistently higher O_2 concentrations and production rates in submerged sediments compared to sediments exposed to air, in agreement with the observations of Haro et al. (2019b). However, the mechanisms underlying this pattern remain poorly understood and no clear mechanistic explanation has yet been established.

Several processes may contribute to the enhanced photosynthetic activity under submerged conditions. One possible explanation, suggested by Cook and Røy (2006), is that sediment submersion increases the availability of dissolved CO_2 for MPB cells, thereby stimulating photosynthesis by approximately 20 %. In addition, submersion provides continuous access to dissolved nutrients such as nitrate and phosphate, which may further support primary production. Physical changes in the sediment may also play a role. For example, Lara et al. (2018) observed reduced porewater content and compaction of the surface sediment during emersion, which could alter the vertical distribution of MPB and consequently their access to light. However, the relative importance of these biogeochemical and physical factors remains unclear and requires further investigation.

In our model, the observed differences between submerged and emersed conditions are represented empirically through a modified O_2 diffusivity combined with a productivity adjustment function (Eq. 8). Although this approach successfully reproduces the measured differences, it does not explicitly resolve the underlying mechanisms and should therefore be regarded as a pragmatic parameterization rather than a process-based representation.

4.6 Model applicability and future development

The model developed in the present study provides a new way to extract primary production parameters from microsensor measurements by explicitly accounting for vertical light attenuation and MPB biomass distributions in intact sediments. Current methods for quantifying benthic primary production include ^{13}C or ^{14}C incubation (often performed on surficial sediment samples that are homogenized or suspended in seawater), closed chamber-based methods, or microsensor-based approaches, each with its benefits and limitations (Revsbech et al., 1981). These methods yield results in the form of gross or net primary production, making comparisons difficult. For example, chamber-based measurements of O_2 exchange rates across the SWI can be confounded by animal respiration (Glud and Blackburn, 2002), while P-I response parameters derived from ^{14}C or ^{13}C uptake in sediments dispersed in water lack the biofilm's natural gradients (Cibic et al., 2008; Brinkman et al., 2015). Microsensor-based methods allow detailed analysis of photosynthesis and O_2 consumption (Revsbech and Jørgensen, 1983; Kühl et al., 1996), but previous studies commonly derived P-I relationships by relating depth-integrated gross production to the incident light intensity at the sediment surface. While this approach describes the apparent productivity response of the biofilm as a whole, it does not resolve how the local production response varies with depth. By combining light attenuation with an

https://doi.org/10.5194/egusphere-2026-4452
Preprint. Discussion started: 28 July 2026

assumed vertical distribution of MPB biomass, our model estimates depth-resolved O_2 production while using a single set of photosynthetic response parameters to represent the MPB community as a whole.

Upscaling of the present model, for example to study primary production across larger systems such as intertidal flats, presents some challenges. The primary limitation are the microsensor measurements, which are used for model calibration. These measurements capture production at a single point, making extrapolation difficult due to the high degree of spatial heterogeneity of intertidal sediments (Glud, 2008). Additionally, acquisition of a comprehensive microsensor data set requires at least 30 min, which limits the ability to collect representative amount of data in a constrained time frame. Variability in additional relevant factors, such as the carbon-to-chlorophyll-*a* ratio, is another potential source of uncertainty.

Nonetheless, by implementing a combination of mechanistic and empirical formulations, our model allows a quantitative assessment of the contributions of different O_2 production and consumption pathways to the overall O_2 budgets in intertidal sediments. Additionally, by representing MPB as a vertically mobile oxygen source and using established equations to capture the effects of irradiance, temperature, and emersion on MPB productivity, our model is transferable to intertidal sediments in other locations. Advances in automated microprofiling technology (Meresse et al., 2023) now enable faster data acquisition under controlled conditions, which significantly improves data collection. When combined with our model, this technology can provide a powerful framework for investigating sediment O_2 dynamics with high spatial and temporal resolution.

Currently, the model is one-dimensional and does not consider lateral processes along tidal gradients or advective transport processess that impact sediment O_2 dynamics in more permeable sediments, such as wave-driven porewater exchange (Precht and Huettel, 2003; Precht et al., 2004), bioturbation and bioirrigation (Polerecky et al., 2006; Meysman et al., 2006; Volkenborn et al., 2007). Future developments could incorporate these aspects. Given the critical role of O_2 fluctuations in coastal biogeochemical cycles (Fusi et al., 2023), expanding the model to a larger spatial and seasonal scale would allow for more comprehensive assessments of carbon, nitrogen, and phosphorus budgets under various climate scenarios.

5 Conclusions

This study provides a process-based framework for simulating O_2 dynamics in the upper layer of MPB-inhabited intertidal sediments under varying light, temperature, and tidal conditions. By combining mechanistic process descriptions with high-resolution microsensor measurements, the model links observed O_2 concentration and gross photosynthesis profiles to the underlying biogeochemical processes controlling oxygen production and consumption.

Application of the model to muddy sediments from the Oosterschelde tidal bay provides new insight into the functioning of this MPB community. Our analysis indicates that the community is adapted to low irradiance and responds to changes in incident light through vertical migration. It further shows that the dominant pathways of sediment O_2 consumption shift with environmental conditions, with reoxidation dominating at low irradiance, aerobic mineralization becoming increasingly important at higher irradiance, and photorespiration representing an additional oxygen sink under high light conditions. The cardinal function adequately describes the temperature response of both oxygen-producing and oxygen-consuming processes across the investigated temperature range.

https://doi.org/10.5194/egusphere-2026-4452
Preprint. Discussion started: 28 July 2026

The model is released as an open-source tool that can be further developed and adapted to other intertidal sediment systems through appropriate parameterization. Future measurements covering a broader range of sediment types, geographical locations, and seasons will allow improved parameter estimation, broader model validation, and increased predictive capability.

Code and data availability. The reaction–transport model presented in this study is openly available as two R packages. *O2DIA*, which provides a command-line interface for model simulations, is archived at Zenodo (Soetaert et al., 2025a) (https://doi.org/10.5281/zenodo.17203645). *O2DIAshiny*, which provides a graphical user interface, is archived separately at Zenodo (Soetaert et al., 2025b) (https://doi.org/10.5281/zenodo.17203649). The experimental data supporting the findings of this study, together with the model documentation, are available in the *O2DIA* Zenodo archive.

Author contributions. QL contributed to the conceptualization, investigation, formal analysis, methodology, software development, visualization, and writing of the original draft. KS contributed to methodology, software development, supervision, funding acquisition, and writing – review and editing. LH contributed to the investigation and formal analysis. VPR contributed to the investigation and formal analysis. LP contributed to the investigation, formal analysis, methodology, software development, supervision, funding acquisition, and writing – review and editing. All authors contributed to the interpretation and discussion of the results, reviewed the manuscript, and approved the submitted version.

Competing interests. The authors declare no conflicts of interest relevant to this study.

Acknowledgements. This study was supported by a UU–NIOZ collaboration project entitled “Impact of microphytobenthos on C, N, P and Si cycling in dynamic intertidal systems” awarded to LP and KS. We thank Lars F. Rickelt (ZENZOR, Denmark) for supplying the scalar irradiance microprobe, Dr. Judith Klatt (Philipps-Universität Marburg & Max Planck Institute for Terrestrial Microbiology, Germany) for kindly lending the fiber-optic spectrometer, and Anton Tramper (NIOZ-Yerseke) for his valuable assistance with sediment sampling and for conducting a large number of microsensor measurements. We further acknowledge support from the Microbahia II project (CTM2017-82274-R) and the FEDER-UCA18-107225 project, which supported Valle Perez-Rodriguez’s research stay at NIOZ and the work conducted during this period.

https://doi.org/10.5194/egusphere-2026-4452
Preprint. Discussion started: 28 July 2026

References

Al-Najjar, M. A., De Beer, D., Jørgensen, B. B., Kühl, M., and Polerecky, L.: Conversion and conservation of light energy in a photosynthetic microbial mat ecosystem, The ISME Journal, 4, 440–449, https://doi.org/10.1038/ismej.2009.121, 2010.

Al-Najjar, M. A., de Beer, D., Kühl, M., and Polerecky, L.: Light utilization efficiency in photosynthetic microbial mats, Environmental Microbiology, 14, 982–992, https://doi.org/10.1111/j.1462-2920.2011.02676.x, 2012.

Allakhverdiev, S. I., Kreslavski, V. D., Klimov, V. V., Los, D. A., Carpentier, R., and Mohanty, P.: Heat stress: an overview of molecular responses in photosynthesis, Photosynthesis research, 98, 541–550, https://doi.org/10.1007/s11120-008-9331-0, 2008.

Apel, K. and Hirt, H.: Reactive oxygen species: metabolism, oxidative stress, and signal transduction, Annu. Rev. Plant Biol., 55, 373–399, https://doi.org/10.1146/annurev.arplant.55.031903.141701, 2004.

Baklouti, M., Diaz, F., Pinazo, C., Faure, V., and Quéguiner, B.: Investigation of mechanistic formulations depicting phytoplankton dynamics for models of marine pelagic ecosystems and description of a new model, Progress in Oceanography, 71, 1–33, https://doi.org/10.1016/j.pocean.2006.05.002, 2006.

Barranguet, C., Kromkamp, J., and Peene, J.: Factors controlling primary production and photosynthetic characteristics of intertidal microphytobenthos, Marine Ecology Progress Series, 173, 117–126, https://doi.org/10.3354/meps173117, 1998.

Berg, P., Risgaard-Petersen, N., and Rysgaard, S.: Interpretation of measured concentration profiles in sediment pore water, Limnology and Oceanography, 43, 1500–1510, https://doi.org/10.4319/lo.1998.43.7.1500, 1998.

Bernard, O. and Rémond, B.: Validation of a simple model accounting for light and temperature effect on microalgal growth, Bioresource technology, 123, 520–527, https://doi.org/10.1016/j.biortech.2012.07.022, 2012.

Berry, J. and Bjorkman, O.: Photosynthetic response and adaptation to temperature in higher plants, Annual Review of plant physiology, 31, 491–543, https://doi.org/10.1146/annurev.pp.31.060180.002423, 1980.

Blackford, J.: The influence of microphytobenthos on the Northern Adriatic ecosystem: a modelling study, Estuarine, Coastal and Shelf Science, 55, 109–123, https://doi.org/10.1006/ecss.2001.0890, 2002.

Borger, E. D., Tiano, J., Braeckman, U., Ysebaert, T., and Soetaert, K.: Biological and biogeochemical methods for estimating bioirrigation: a case study in the Oosterschelde estuary, Biogeosciences, 17, 1701–1715, https://doi.org/10.5194/bg-17-1701-2020, 2020.

Boudreau, B. P. and Jørgensen, B. B., eds.: The Benthic Boundary Layer: Transport Processes and Biogeochemistry, Oxford University Press, New York, USA, ISBN 9780195118810, https://doi.org/10.1093/oso/9780195118810.001.0001, 2001.

Brinkman, A. G., Riegman, R., Jacobs, P., Kuhn, S., and Meijboom, A.: Ems-Dollard primary production research: Full data report, Tech. Rep. C160/14, IMARES Wageningen UR, IJmuiden, the Netherlands, https://www.vliz.be/imisdocs/publications/ocrd/356865.pdf, 2015.

Canfield, D. E., Kristensen, E., and Thamdrup, B.: Aquatic geomicrobiology, Gulf Professional Publishing, 2005.

Cibic, T., Blasutto, O., Burba, N., and Umani, S. F.: Microphytobenthic primary production as 14C uptake in sublittoral sediments of the Gulf of Trieste (northern Adriatic Sea): methodological aspects and data analyses, Estuarine, Coastal and Shelf Science, 77, 113–122, https://doi.org/10.1016/j.ecss.2007.09.005, 2008.

Cloern, J. E., Grenz, C., and Vidergar-Lucas, L.: An empirical model of the phytoplankton chlorophyll: carbon ratio-the conversion factor between productivity and growth rate, Limnology and Oceanography, 40, 1313–1321, https://doi.org/10.4319/lo.1995.40.7.1313, 1995.

Cook, P. L. and Røy, H.: Advective relief of CO2 limitation in microphytobenthos in highly productive sandy sediments, Limnology and Oceanography, 51, 1594–1601, https://doi.org/10.4319/lo.2006.51.4.1594, 2006.

https://doi.org/10.5194/egusphere-2026-4452
Preprint. Discussion started: 28 July 2026

Costache, T., Acien Fernandez, F. G., Morales, M., Fernández-Sevilla, J., Stamatin, I., and Molina, E.: Comprehensive model of microalgae photosynthesis rate as a function of culture conditions in photobioreactors, Applied microbiology and biotechnology, 97, 7627–7637, https://doi.org/10.1007/s00253-013-5035-2, 2013.

Cussler, E. L.: Diffusion: mass transfer in fluid systems, Cambridge university press, 2009.

De Jonge, V.: Fluctuations in the organic carbon to chlorophyll a ratios for estuarine benthic diatom populations, Mar. Ecol. Prog. Ser, 2, 345–353, https://doi.org/10.3354/meps002345, 1980.

Eilers, P. and Peeters, J.: A model for the relationship between light intensity and the rate of photosynthesis in phytoplankton, Ecological modelling, 42, 199–215, https://doi.org/10.1016/0304-3800(88)90057-9, 1988.

Fusi, M., Rigaud, S., Guadagnini, G., Barausse, A., Marasco, R., Daffonchio, D., Régis, J., Huchet, L., Camin, C., Pettit, L., Vina-Herbon, C., and Giomi, F.: Ideas and perspectives: The fluctuating nature of oxygen shapes the ecology of aquatic habitats and their biogeochemical cycles – the aquatic oxyscape, Biogeosciences, 20, 3509–3521, https://doi.org/10.5194/bg-20-3509-2023, 2023.

Geider, R., MacIntyre, H., and Kana, T.: Dynamic model of phytoplankton growth and acclimation: responses of the balanced growth rate and the chlorophyll a: carbon ratio to light, nutrient-limitation and temperature, Marine Ecology Progress Series, 148, 187–200, https://doi.org/10.3354/meps148187, 1997.

Giomi, F., Barausse, A., Steckbauer, A., Daffonchio, D., Duarte, C. M., and Fusi, M.: Oxygen dynamics in marine productive ecosystems at ecologically relevant scales, Nature Geoscience, 16, 560–566, https://doi.org/10.1038/s41561-023-01217-z, 2023.

Giordano, M., Beardall, J., and Raven, J. A.: CO 2 concentrating mechanisms in algae: mechanisms, environmental modulation, and evolution, Annu. Rev. Plant Biol., 56, 99–131, https://doi.org/10.1146/annurev.arplant.56.032604.144052, 2005.

Glud, R. N.: Oxygen dynamics of marine sediments, Marine Biology Research, 4, 243–289, https://doi.org/10.1080/17451000801888726, 2008.

Glud, R. N. and Blackburn, N.: The effects of chamber size on benthic oxygen uptake measurements: a simulation study, Ophelia, 56, 23–31, https://doi.org/10.1080/00785236.2002.10409486, 2002.

Glud, R. N., Ramsing, N. B., and Revsbech, N. P.: PHOTOSYNTHESIS AND PHOTOSYNTHESIS-COUPLED RESPIRATION IN NATURAL BIOFILMS QUANTIFIED WITH OXYGEN MICROSENSORS 1, Journal of Phycology, 28, 51–60, https://doi.org/10.1111/j.0022-3646.1992.00051.x, 1992.

Guarini, J.-M., Blanchard, G., Gros, P., Gouleau, D., and Bacher, C.: Dynamic model of the short-term variability of microphytobenthic biomass on temperate intertidal mudflats, Marine Ecology Progress Series, 195, 291–303, https://doi.org/10.3354/meps195291, 2000.

Han, B.-P.: A mechanistic model of algal photoinhibition induced by photodamage to photosystem-II, Journal of theoretical biology, 214, 519–527, https://doi.org/10.1006/jtbi.2001.2468, 2002.

Hancke, K. and Glud, R. N.: Temperature effects on respiration and photosynthesis in three diatom-dominated benthic communities, Aquatic Microbial Ecology, 37, 265–281, https://doi.org/10.3354/ame037265, 2004.

Haro, S., Bohórquez, J., Lara, M., Garcia-Robledo, E., González, C., Crespo, J., Papaspyrou, S., and Corzo, A.: Diel patterns of microphytobenthic primary production in intertidal sediments: the role of photoperiod on the vertical migration circadian rhythm, Scientific Reports, 9, 13 376, https://doi.org/10.1038/s41598-019-49971-8, 2019a.

Haro, S., Brodersen, K., Bohórquez, J., Papaspyrou, S., Corzo, A., and Kühl, M.: Radiative energy budgets in a microbial mat under different irradiance and tidal conditions, Microbial ecology, 77, 852–865, https://doi.org/10.1007/s00248-019-01350-6, 2019b.

Havaux, M.: Rapid photosynthetic adaptation to heat stress triggered in potato leaves by moderately elevated temperatures, Plant, Cell & Environment, 16, 461–467, https://doi.org/10.1111/j.1365-3040.1993.tb00893.x, 1993.

https://doi.org/10.5194/egusphere-2026-4452
Preprint. Discussion started: 28 July 2026

Hewitt, J. E., Ellis, J. I., and Thrush, S. F.: Multiple stressors, nonlinear effects and the implications of climate change impacts on marine coastal ecosystems, Global change biology, 22, 2665–2675, https://doi.org/10.1111/gcb.13176, 2016.

Hochard, S., Pinazo, C., Grenz, C., Evans, J. L. B., and Pringault, O.: Impact of microphytobenthos on the sediment biogeochemical cycles: A modeling approach, Ecological Modelling, 221, 1687–1701, https://doi.org/10.1016/j.ecolmodel.2010.04.002, 2010.

Ippoliti, D., Gómez, C., del Mar Morales-Amaral, M., Pistocchi, R., Fernández-Sevilla, J., and Acién, F. G.: Modeling of photosynthesis and respiration rate for Isochrysis galbana (T-Iso) and its influence on the production of this strain, Bioresource Technology, 203, 71–79, https://doi.org/10.1016/j.biortech.2015.12.050, 2016.

Jørgensen, B. B. and Des Marais, D. J.: A simple fiber-optic microprobe for high resolution light measurements: application in marine sediment., Limnology and Oceanography, 31, 1376–1383, https://doi.org/10.4319/lo.1986.31.6.1376, 1986.

Kromkamp, J. C. and Forster, R. M.: The use of variable fluorescence measurements in aquatic ecosystems: differences between multiple and single turnover measuring protocols and suggested terminology, European Journal of Phycology, 38, 103–112, https://doi.org/10.1080/0967026031000094094, 2003.

Kühl, M. and Jørgensen, B. B.: Spectral light measurements in microbenthic phototrophic communities with a fiber-optic microprobe coupled to a sensitive diode array detector, Limnology and Oceanography, 37, 1813–1823, https://doi.org/10.4319/lo.1992.37.8.1813, 1992.

Kühl, M. and Jørgensen, B. B.: The light field of microbenthic communities: radiance distribution and microscale optics of sandy coastal sediments, Limnology and oceanography, 39, 1368–1398, https://doi.org/10.4319/lo.1994.39.6.1368, 1994.

Kühl, M., Lassen, C., and Jørgensen, B. B.: Light penetration and light intensity in sandy marine sediments measured with irradiance and scalar irradiance fiber-optic microprobes, Marine Ecology Progress Series, 105, 139–148, https://doi.org/10.3354/meps105139, 1994.

Kühl, M., Glud, R. N., Ploug, H., and Ramsing, N. B.: Microenvironmental control of photosynthesis and photosynthesis-coupled respiration in an epilithic cyanobacterial biofilm 1, Journal of Phycology, 32, 799–812, https://doi.org/10.1111/j.0022-3646.1996.00799.x, 1996.

Lara, M., Bohorquez, J., Jiménez-Arias, J. L., María Crespo, J., Haro, S., Papaspyrou, S., García-Robledo, E., Meysman, F., and Corzo, A.: Microscale drivers of oxygen dynamics during emersion: Microphytobenthic production, sediment compaction and shifts on diffusivity., in: EGU General Assembly Conference Abstracts, p. 19488, 2018.

Lassen, C., Ploug, H., and Jørgensen, B. B.: A fibre-optic scalar irradiance microsensor: application for spectral light measurements in sediments, FEMS Microbiology Letters, 86, 247–254, https://doi.org/10.1016/0378-1097(92)90788-p, 1992.

Liu, Q., Polerecky, L., Rios-Yunes, D., and Soetaert, K.: Simulating the thermal response of tidal sediments by integrating numerical modeling and field measurements, Journal of Geophysical Research: Oceans, 130, e2025JC023 263, https://doi.org/10.1029/2025jc023263, 2025.

Malkin, S. Y. and Meysman, F.: Rapid redox signal transmission by âœcable bacteriaâ beneath a photosynthetic biofilm, Applied and environmental microbiology, 81, 948–956, https://doi.org/10.1128/aem.02682-14, 2015.

Mariotti, G. and Fagherazzi, S.: Modeling the effect of tides and waves on benthic biofilms, Journal of Geophysical Research: Biogeosciences, 117, 2012JG002 064, https://doi.org/10.1029/2012jg002064, 2012.

Meresse, M., Gevaert, F., Duong, G., and Denis, L.: A new procedure for autonomous acquisition of photosynthesis-irradiance curves on a microphytobenthic biofilm, Frontiers in Marine Science, 10, 1167 464, https://doi.org/10.3389/fmars.2023.1167464, 2023.

Meysman, F. J., Galaktionov, O. S., Gribsholt, B., and Middelburg, J. J.: Bioirrigation in permeable sediments: Advective pore-water transport induced by burrow ventilation, Limnology and Oceanography, 51, 142–156, https://doi.org/10.4319/lo.2006.51.1.0142, 2006.

Mittler, R.: Oxidative stress, antioxidants and stress tolerance, Trends in plant science, 7, 405–410, https://doi.org/10.1016/s1360-1385(02)02312-9, 2002.

https://doi.org/10.5194/egusphere-2026-4452
Preprint. Discussion started: 28 July 2026

Nmor, S. I.: Modelling microphytobenthos contribution and tidal effect on sediment biogeochemistry, Master's thesis, Ghent University, 2020.

Polerecky, L., Volkenborn, N., and Stief, P.: High temporal resolution oxygen imaging in bioirrigated sediments, Environmental Science & Technology, 40, 5763–5769, https://doi.org/10.1021/es060494l, 2006.

Precht, E. and Huettel, M.: Advective pore-water exchange driven by surface gravity waves and its ecological implications, Limnology and Oceanography, 48, 1674–1684, https://doi.org/10.4319/lo.2003.48.4.1674, 2003.

Precht, E., Franke, U., Polerecky, L., and Huettel, M.: Oxygen dynamics in permeable sediments with wave-driven pore water exchange, Limnology and Oceanography, 49, 693–705, https://doi.org/10.4319/lo.2004.49.3.0693, 2004.

R Core Team: R: A Language and Environment for Statistical Computing, R Foundation for Statistical Computing, Vienna, Austria, https://www.R-project.org/, 2023.

Rakotomalala, C., Guizien, K., Grangeré, K., Lefebvre, S., Dupuy, C., and Orvain, F.: Modelling the functioning of a coupled microphytobenthic-EPS-bacterial system in intertidal mudflats, Marine environmental research, 150, 104 754, https://doi.org/10.1016/j.marenvres.2019.104754, 2019.

Revsbech, N. P.: An oxygen microsensor with a guard cathode, Limnology and Oceanography, 34, 474–478, https://doi.org/10.4319/lo.1989.34.2.0474, 1989.

Revsbech, N. P. and Jørgensen, B. B.: Photosynthesis of benthic microflora measured with high spatial resolution by the oxygen microprofile method: capabilities and limitations of the method 1, Limnology and Oceanography, 28, 749–756, https://doi.org/10.4319/lo.1983.28.4.0749, 1983.

Revsbech, N. P., Jørgensen, B. B., and Brix, O.: Primary production of microalgae in sediments measured by oxygen microprofile, H14CO3-fixation, and oxygen exchange methods 1, Limnology and Oceanography, 26, 717–730, https://doi.org/10.4319/lo.1981.26.4.0717, 1981.

Rios-Yunes, D., Tiano, J. C., van Oevelen, D., van Dalen, J., and Soetaert, K.: Annual biogeochemical cycling in intertidal sediments of a restored estuary reveals dependence of N, P, C and Si cycles to temperature and water column properties, Estuarine, Coastal and Shelf Science, 282, 108 227, https://doi.org/10.1016/j.ecss.2023.108227, 2023.

Rosso, L., Lobry, J. R., and Flandrois, J.-P.: An unexpected correlation between cardinal temperatures of microbial growth highlighted by a new model, Journal of theoretical biology, 162, 447–463, https://doi.org/10.1006/jtbi.1993.1099, 1993.

Sanchez Zurano, A., Gomez Serrano, C., Acién-Fernández, F. G., Fernández-Sevilla, J. M., and Molina-Grima, E.: Modeling of photosynthesis and respiration rate for microalgae–bacteria consortia, Biotechnology and Bioengineering, 118, 952–962, https://doi.org/10.1002/bit.27625, 2021.

Santschi, P., Höhener, P., Benoit, G., and Buchholtz-ten Brink, M.: Chemical processes at the sediment-water interface, Marine chemistry, 30, 269–315, https://doi.org/10.1016/0304-4203(90)90076-o, 1990.

Savelli, R., Dupuy, C., Barillé, L., Lerouxel, A., Guizien, K., Philippe, A., Bocher, P., Polsenaere, P., and Le Fouest, V.: On biotic and abiotic drivers of the microphytobenthos seasonal cycle in a temperate intertidal mudflat: a modelling study, Biogeosciences, 15, 7243–7271, https://doi.org/10.5194/bg-15-7243-2018, 2018.

Serôdio, J. and Catarino, F.: Modelling the primary productivity of intertidal microphytobenthos: time scales of variability and effects of migratory rhythms, Marine Ecology Progress Series, 192, 13–30, https://doi.org/10.3354/meps192013, 2000.

Serôdio, J., Vieira, S., Cruz, S., and Barroso, F.: Short-term variability in the photosynthetic activity of microphytobenthos as detected by measuring rapid light curves using variable fluorescence, Marine Biology, 146, 903–914, https://doi.org/10.1007/s00227-004-1504-6, 2005.

https://doi.org/10.5194/egusphere-2026-4452
Preprint. Discussion started: 28 July 2026

Serôdio, J., Coelho, H., Vieira, S., and Cruz, S.: Microphytobenthos vertical migratory photoresponse as characterised by light-response curves of surface biomass, Estuarine, Coastal and Shelf Science, 68, 547–556, https://doi.org/10.1016/j.ecss.2006.03.005, 2006.

Soetaert, K.: rootSolve: Nonlinear Root Finding, Equilibrium and Steady-State Analysis of Ordinary Differential Equations, CRAN [code], https://doi.org/10.32614/CRAN.package.rootSolve, 2023.

Soetaert, K. and Meysman, F.: Reactive transport in aquatic ecosystems: Rapid model prototyping in the open source software R, Environmental Modelling & Software, 32, 49–60, https://doi.org/10.1016/j.envsoft.2011.08.011, 2012.

Soetaert, K., Herman, P. M., and Middelburg, J. J.: A model of early diagenetic processes from the shelf to abyssal depths, Geochimica et Cosmochimica Acta, 60, 1019–1040, https://doi.org/10.1016/0016-7037(96)00013-0, 1996.

Soetaert, K., Petzoldt, T., and Meysman, F.: marelac: Tools for Aquatic Sciences, CRAN [code], https://doi.org/10.32614/CRAN.package.marelac, 2010a.

Soetaert, K., Petzoldt, T., and Setzer, R. W.: Solving differential equations in R: package deSolve, Journal of statistical software, 33, 1–25, https://doi.org/10.18637/jss.v033.i09, 2010b.

Soetaert, K., Liu, Q., and Polerecky, L.: O2DIA/O2DIA: release v1.0.0 on 9/25/2025 (v1.0.0), https://doi.org/10.5281/zenodo.17203645, 2025a.

Soetaert, K., Liu, Q., and Polerecky, L.: O2DIA/O2DIAshiny: release v1.0.0 on 9/25/2025 (v1.0.0), https://doi.org/10.5281/zenodo.17203649, 2025b.

Volkenborn, N., Polerecky, L., Hedtkamp, S., van Beusekom, J. E., and De Beer, D.: Bioturbation and bioirrigation extend the open exchange regions in permeable sediments, Limnology and Oceanography, 52, 1898–1909, https://doi.org/10.4319/lo.2007.52.5.1898, 2007.